Tools for uranium characterization in carbonate samples: Case studies of natural U-Pb geochronology reference materials

E Troy Rasbury[1], Theodore M Present[2], Paul Northrup[1], Ryan V Tappero[3], Antonio Lanzirotti[4], Jennifer M Cole[5,6], Kathleen M Wooton[1], and Kevin Hatton[1]

[1]Department of Geosciences, FIRST, Stony Brook University, 100 Nichols Rd, Stony Brook, NY 11794, USA
[2]Division of Geological and Planetary Sciences, California Institute of Technology, 307 North Mudd Laboratory, Pasadena, CA 91125, USA
[3]NSLS-II, Brookhaven National Laboratory, Upton NY 11973, USA
[4]Center for Advanced Radiation Sources, Randall, Chicago, IL 60637
[5]Department of Science, West Los Angeles College, Culver City, CA 90230, USA
[6]Lamont-Doherty Earth Observatory of Columbia University, 61 Route 9W, Palisades, NY 10964, USA

Correspondence: E. Troy Rasbury (troy.rasbury@stonybrook.edu))

Abstract. Laser ablation U-Pb analyses of carbonate (LAcarb) samples has greatly expanded the potential for U-Pb dating to a variety of carbonate producing settings. Carbonates that were previously considered impossible to date using isotope dilution methods may preserve radiogenic domains that can be dated using spatially resolved laser ablation geochronology techniques. Work is ongoing to identify reference materials and to consider best practices for LAcarb. In this study we apply standard and emerging characterization toolsets on three natural samples with the dual goal of enhancing the study of carbonates and in establishing a new set of well characterized natural reference materials for LAcarb studies. We start with the existing carbonate reference material WC-1 from the Permian Reef Complex of Texas, building on the published description to offer a deeper look at U and associated trace elements. We consider a tufa sample from the Miocene Barstow Formation of the Mojave Block, California, as a possible secondary calcite reference material due to its well-behaved U-Pb systematics. There are currently no natural dolomite standards. We present an unusual dolomite sample with very well-behaved U-Pb systematics from the Miocene of the Turkana Basin of Kenya as a possible dolomite reference material for LAcarb dating. In addition to using XRF mapping and spectroscopy to better understand U in these natural samples, we have analyzed multiple aliquots of each of them for $^{87}Sr/^{86}Sr$ by TIMS. The Sr isotope compositions are analytically homogeneous within petrographically-homogeneous regions of all three samples, so these materials could be used as Sr isotope standards as well. While not part of the current contribution, this combination could streamline simultaneous LA analyses of $^{87}Sr/^{86}Sr$ and U-Pb geochronology.

1 Introduction

Carbonates are ubiquitous in the Earth's crust and form from a variety of fluids, often with characteristic isotopic and element ratios (Fig. 1). Carbonate producing fluids in all crustal levels range from oxygenated to reducing, from low salinity to high salinity and from low temperature to high temperature. Fluids evolve as they interact with rocks along their flow paths, adding complexity, but also providing opportunities to trace these processes with the rock's paragenetic history. Carbonate compo-

sitions are highly susceptible to diagenetic alteration, particularly when fluid chemistry and temperature changes affect the thermodynamic stability of carbonate minerals. Mixing of fluids can be particularly corrosive such as seen where seawater and fresh water mix in a carbonate platform, or can be responsible for mineral precipitation depending on the saturation state of the combined fluids (Runnells, 1969; Wigley and Plummer, 1976). Thus, introduction of fluids with different chemistries through exposure, uplift, or burial can destroy the original carbonate prior to precipitation of a new carbonate or can alter the carbonates visibly or at a microscopic scale. Therefore, an important part of investigation of carbonates should involve establishing field and petrographic relationships. Standard assessment of field and petrographic relationships between carbonate phases is a prerequisite to developing a detailed rock paragenesis necessary for interpreting the timing and source of depositional and diagenetic fluids interacting with carbonate rocks. Here, we present tools useful for characterizing the incorporation of radiogenic elements–especially uranium, lead, and strontium–into carbonates as a means for relating $^{87}Sr/^{86}Sr$ and U/Pb data to carbonate paragenetic frameworks.

It is widely recognized that carbonates are a proxy for the fluids that formed them. Published studies demonstrate the need for careful characterization of carbonates in order to interpret geochemical results in geologically meaningful context, and this same attention to detail is needed to understand U-Pb results. Carbonates have element ratios that are controlled by the composition of the fluid and the partition coefficient (Kd) of the element for the crystal lattice (Banner and Hanson, 1990). Special circumstances are required to have elevated U in calcite because the Kd is less than 0.05 (Reeder et al., 2001; Drysdale et al., 2019; Weremeichik et al., 2017). However, aragonite, which is metastable, does not exclude U. (Reeder et al., 2001) and Kelly et al. (2003) suggested that high U contents in a speleothem calcite (which we use as a U(VI) standard), might have been inherited from high concentrations in primary aragonite and preserved during neomorphic inversion to calcite. No experimental studies for U incorporation have been reported for dolomite, but it is unlikely to have a higher affinity for U than calcite as they have the similar structures and there is more of a size mismatch with Mg than Ca. Using modern settings and a laboratory understanding of trace element incorporation, we know that U incorporation follows aragonite > high Mg calcite> calcite (Chung and Swart, 1990; Reeder et al., 2001). Seawater has elevated U/Pb, but carbonates forming from seawater have much lower U/Pb, demonstrating that the structure has a much higher affinity for Pb than U (Shen and Boyle, 1988), at least at seawater composition.

No lab experiments have studied U^{4+} incorporation in carbonates, despite several published examples of natural carbonates with reduced U (Sturchio, 1998; Cole et al., 2004) and an additional example we present in this contribution. Because U^{4+} is immobile in most aqueous fluids, carbonate minerals that incorporate U^{4+} must represent precipitates from poorly-understood fluid compositions in depositional or diagenetic environments. Recent work on modern calcite from a deep granite aquifer with reducing fluids is suggesting a mechanism for U^{4+} transport (Drake et al., 2018). Experimental work at elevated T has shown that $U(IV)Cl_40$ is soluble in acid solutions (Timofeev et al., 2018), and high T experiments of U in hydrocarbons indicate that economic concentrations can be produced via transport in hydrocarbons (Migdisov et al., 2017), but how would these processes result in incorporation in carbonates? There is likely more than one mechanism and this is a fruitful avenue for future research both of synthetic and natural carbonate samples. Understanding U incorporation in carbonates is important for a holistic approach to U-Pb dating, but there is no evidence that the oxidation state of U in carbonates has any control on the

reliability of the dating. However, understanding U speciation might elucidate the depositional or diagenetic condition under which the U was incorporated, and therefore affect the interpretation of the U/Pb date.

Cement stratigraphy is a powerful approach to establish the relative age relationships of carbonate phases, or paragenesis across a basin. This approach uses relative relationships of cements from the thin section scale and correlation of these throughout a basin or region (Meyers, 1991, 1974). This field to petrographic approach has been used to select samples for geochemistry, providing fundamental insights into the fluid evolution of basins and degree of rock/water interaction e.g. (Banner and Hanson, 1990), as well as establishing trace and minor element incorporation trends (e.g., Mn/Fe) useful for tracking burial histories (Barnaby and Rimstidt, 1989). Often, combining microanalytical tools that characterize carbonates at the micron to centimeter scale of cement growth zones is required to understand the origin and timing of various textures in complex samples. Chemical imaging techniques, carbonate staining, and polarized light, fluorescence, electron, and cathodoluminescence microscopy provide spatial context for quantitative microscale analyses of fluid inclusion, ion microprobe, electron microprobe, and laser ablation measurements. Integrated data from such a toolkit enables collection of LA-U-Pb isochrons that reliably dates a single paragenetic event and permits geologically meaningful interpretation of U-Pb ages. U-Pb dating in this context places age constraints on the fluids which can then be tied to testable hypothesis about the origin and changes in the fluids whatever the technique for dating is (Lawson et al., 2018; Quade et al., 2017; Parrish et al., 2019; Pisapia et al., 2018; Woodhead et al., 2010; Winter and Johnson, 1995; Hoff et al., 1995; Cole et al., 2005; Polyak et al., 2008, 2013; Luczaj and Goldstein, 2000; Brannon et al., 1996; Godeau et al., 2018; Rasbury et al., 2004, 1997; Pagel et al., 2018; Roberts et al., 2020).

Laser ablation mapping (Woodhead et al., 2010, 2007; Piccione et al., 2019; Drost et al., 2018; Roberts et al., 2020), synchrotron XRF mapping (Cole et al., 2004; Piccione et al., 2019; Frisia et al., 2008; Vanghi et al., 2019), PIXE (Ortega et al., 2005, 2003) μXRF (de Winter et al., 2017), and EMPA (Suzuki et al., 2016) permit tying petrographic observations of different phases to in situ chemical maps of U and other elements that inform fluid chemistry. For the purpose of U-Pb dating, knowledge of the mineral lattice location of U and it's oxidation state and speciation provide a fundamental framework for interpreting ages as well as revealing details of the fluid chemistry (Kelly et al., 2006, 2003; Sturchio, 1998; Cole et al., 2004). In some cases, uranium minerals are encapsulated in calcite which can protect them from alteration Suzuki et al. (2016); Ludwig (1978).

Given that the major element composition of seawater has changed appreciably through time (Hardie, 1996; Lowenstein, 2001; Horita et al., 2002), that meteoric fluid compositions are controlled by water rock interaction (Chung and Swart, 1990; Banner and Hanson, 1990) and that deep brines have evolved since deposition in basins (Musgrove and Banner, 1993), we can imagine that there is no such thing as a typical fluid. A holistic approach to dating carbonates should involve an effort to see back to the fluid or fluids that have been responsible for its formation and how they might have changed through the diagenetic history. This, particularly in the context of how favorable the U concentrations and U/Pb ratios are, will provide an important path towards understanding factors that create favorable carbonate samples for U-Pb dating. The purpose of this contribution is to highlight tools that are available for carbonate characterization relevant to U-Pb dating. These tools build on the more commonly used petrographic approaches, particularly cathodoluminescence (CL) imaging, such as demonstrated in the three case studies presented here.

1.1 Mapping Uranium

While the U/Pb ratio matters for dating, it is usually the U concentration that limits the potential. Mapping U at low concentrations in carbonates is challenging, but necessary to tie U-Pb ages to paragenetic context and to identify datable phases, so the focus here will be on tools that map the distribution of U on the hand specimen to thin section scale.

Fission track mapping (Chung and Swart, 1990; Hoff et al., 1995; Rasbury et al., 2000; Cole et al., 2004; Becker et al., 2002; Wang et al., 1998; Luczaj and Goldstein, 2000; Amiel et al., 1973; Haglund et al., 1969; Gvirtzman et al., 1973) can help to map the distribution of U on the microscopic to hand specimen scales. This simply requires making a polished slab, placing it on a detector such as Lexan plastic (Chung and Swart, 1990) and sending it to a nuclear reactor. Depending on the flux requested, it typically takes weeks for the samples to be returned due to harmful radioactivity produced in the reactor. Once back, the detector has to be etched to increase the size of the tracks for visibility and then a comparison to the rock can be made. Thin sections can be used, making it easier to relate the tracks to the exact phases. There is a modest cost for sending samples to a reactor, but this is an underutilized non-destructive approach. For samples with high U (10's of ppm), modern high resolution scanners can image the tracks. For lower concentration samples, high magnification microscope images can be stitched together to provide a larger scale framework for the U distribution.

Autoradiography (Cole et al., 2003; Pickering et al., 2011) offers the opportunity to examine radioactive elements on the hand specimen scale. Phosphor imaging plates are used in biomedical and biochemical studies to detect samples tagged with radionuclides. While the scanning devices themselves are somewhat costly, phosphor screens can be rented from imaging centers or even purchased at lower cost, making this technique more broadly applicable. Polished hand samples along with a solid standard are left to activate the phosphor over time (days to weeks), ideally in a shielded environment. Following exposure, the screens are scanned to produce a digital autoradiograph that provides a map of relative differences in U and Th concentrations directly comparable to the hand specimen (Cole et al., 2003; Pickering et al., 2011). Cm-scale regions of higher U (and Th) can then be targeted further with sampling and other finer-scale mapping techniques.

Synchrotron X-ray fluorescence (SXRF) imaging and X-ray absorption spectroscopy (XAS) techniques have the ability to provide information about both the distribution of major and trace elements, including U and Pb, in samples as well as their valence state and speciation. Using XAS methods it is possible to quantify U valence state at concentrations of a few ppm. Synchrotron X-ray beamlines are available through a competitive process of general user proposals (Sutton et al., 2002). These brighter sources offer micron sized resolution for low ppm levels of the elements of interest. Emerging tender energy spectroscopy (TES), using the energy range between soft and hard Xray techniques allows mapping of elements such as Mg and S that are important in carbonates (Northrup, 2019). In addition to XRF maps which show element distribution and the relationships among elements, spots can be chosen for spectroscopy, providing mineralogy (Mg, Ca) and redox (U, Fe, Mn etc).

Bench-top microscale XRF mapping (μXRF) of major, minor, and trace elements by energy-dispersive spectroscopy permits geochemical characterization of samples at the micron to decimeter scale. X-ray focusing optics, rather than collimation, allow high spatial resolutions (ca. 15-25 μm) with laboratory X-ray sources. μXRF has been used for chemical imagining in di-

verse fields, including materials characterization, archaeology, and earth sciences (de Winter et al., 2017; Allwood et al., 2018; Katsuta et al., 2019; **?**; de Winter and Claeys, 2017), and related instruments will be deployed on interplanetary spacecraft (Williford et al., 2018). Qualitative and semi-quantitative imaging and standardless analysis is rapid and versatile, but quantitative composition determination of carbonate rocks is challenging due to the X-ray-transparent carbonate matrix (de Winter et al., 2017). As shown here, in some samples with high U concentrations, U abundance can be mapped with appropriate analytical conditions, such as incident radiation filtering, multiple beam dwell passes, acquisition under vacuum, and preparation of thick samples that permit excitation of all available U atoms through the sample depth. Data presented here was acquired using an M4 Tornado (Bruker) operating with a 30 W Rh x-ray tube excited at 50 kV and focused to a 17 µm spot (1 σ of incident energy at Mo-Kσ) on flat, polished, thick (> 2 mm) samples under 20 mbar vacuum. Fluorescence energy was detected with two 60 mm^2 XFlash silicon drift detectors (Bruker), energy spectra were deconvolved with Bruker software, and total counts in each emission line region were exported for plotting and visualization using MATLAB (Mathworks).

2 Case Studies

We use three natural carbonates that have potential as LAcarb reference materials to illustrate imaging and spectroscopy techniques. We also discuss what is known of the geology and geochemistry to provide context for other samples that might be dated.

2.1 Late Permian Marine Cement- Permian Reef Complex

Roberts et al. (2017) offered WC-1 (Walnut Canyon) as a primary standard for LAcarb. This late Permian marine cement sample is reasonably homogeneous with high enough U/Pb and radiogenic enough Pb isotopes to make it a suitable reference material. A brief description of the field relationships and U-Pb characterization were presented in Roberts et al. (2017), but here we expand on this to offer additional insight into the reference material as well as to highlight characterization techniques that are relevant to any carbonate study. Similar buildups and cements are described from important oil plays in Kazakhstan (Dickson and Kenter, 2014), and comparisons have been made to Precambrian marine aragonite cements (Grotzinger and Knoll, 1995). Cements of this type offer good potential for giving ages of penecontemporaneous marine diagenesis.

The Permian Reef Complex, spectacularly exposed in the Guadalupe Mountains National Park of West Texas, stands in relief primarily due to the type of cements that make up WC-1. Neptunian dikes are found parallel to the reef track, filling fractures that resulted from tensional stresses as the reef built out into the Permian Basin (Hunt et al., 2003; Budd et al., 2013; Frost et al., 2013). Early marine cements in the reef and within these Neptunian dikes are primarily botryoidal aragonites and are typically a dark brown color. The dark brown color is from organic matter that is occluded in the carbonate such that when broken or sawn these cements smell like hydrocarbons (anecdotally this strong smell is a good criterion for selecting carbonates for dating). The cements have mostly been altered to calcite, though Chafetz et al. (2008) found original aragonite in similar cements from the same area. Calcite with the greatest alteration is light brown and has less favorable U/Pb (Jones et al., 1995). Petrograpically these cements preserve details of the original fibrous aragonite as inclusion trails. WC-1 (Walnut

Canyon) comes from a Neptunian dike in the upper Capitan Formation of the Permian Reef Complex, equivalent to the Tansill Formation on the shelf. This Neptunian dike is exposed in Walnut Canyon just outside the Guadalupe Mountains National Park entrance. The botryoids that fill the Neptunian dike were made of radiating aragonite needles that bundle into cm scale packages. The botryoids grow atop one another from both sides of the dike (Fig. 2). At the hand specimen scale, cross-cutting white veins are obvious ((Fig 3). Other veins are smaller but can be detected with petrography and element mapping (Fig. 3). The Permian Reef Complex has seen many episodes of diagenetic fluids, including meteoric fluids accompanying the Basin and Range extension that exhumed the reef in the Neogene (Bishop et al., 2014; Loyd et al., 2013; Scholle et al., 1992; Budd et al., 2013).

Cathodoluminescence (CL) has been a go-to test for diagenesis, and when an activator such as Mn is present, this often gives phenomenal images that illuminate alteration, as well as veins and single crystals in fractures which can track reactivation and changes in the chemistry and rate of fluid flow. However, it is also understood that Fe quenches luminescence, so the Mn/Fe ratio matters for understanding what luminescence or non-luminescence means (Barnaby and Rimstidt, 1989). In the case of Walnut Canyon, the well preserved botryoids are non-luminescent and cements that line the botryoids are brightly luminescent (Fig. 3). Even through the botryoids are non-luminescent with excellent textural preservation, the wide range of Sr concentrations across the botryoids shows that they have been variably altered (Fig.3, Fig. 4, Fig. 5). Element imaging is complimentary to petrography, and while petrographic techniques like CL can provide qualitative information on Mn and Fe, XRF and LA imaging techniques give quantitative information on the Fe/Mn, Sr/Ca and other ratios and element concentrations, providing far more insight into the carbonate diagenesis. μXRF scanning is reasonably accessible, and we suggest that depending on the original mineralogy, elements like Sr (Fig. 3, Fig. 4) could be mapped and registered so that only the best preserved parts of a rock slab could be targeted for a LAcarb reference material. This should greatly reduce the scatter that is currently seen in the WC-1 reference material.

While optical orientation is preserved and fluid inclusions and aragonite relict mineral inclusions delineate the original acicular growth habit, the carbonate is almost entirely replaced by cloudy brown calcite (S. J. Mazzullo, 1980). This neomorphic replacement may facilitate retention of U (Kelly et al., 2003), or perhaps the organic matter (that gives the sample its color and pungent smell when broken) complexed U and retained it in the calcite. Remarkably, Sr is lost well before U in this system as evidenced by the rather homogeneous U concentration at about 4.5 ppm (which makes this a good U-Pb reference material) and the highly variable Sr (Fig. 3). Isotope dilution of this sample doesn't give much of a spread in U/Pb, so to maximize the spread a range of aliquots from dark brown to light brown were utilized (Roberts et al., 2017). Like the result reported in Jones et al. (1995), this produced an age that is nominally younger than the age of the reef based on dating of ash beds (Wu et al., 2020) (254 instead of 257 Ma), but not outside the uncertainty. The cements postdate reef cementation because they fill fractures, but contain internal sediments and likely cemented penecontemporaneously with reef deposition. The $^{87}Sr/^{86}Sr$ ratios range from 0.7069-0.7072 (Fig. 6), with an average of 0.706930(.000069) for samples that make up the bulk of the dike. These values are similar to what Chafetz et al. (2008) reported from samples with primary aragonite from peritidal teepee structures in the correlative Tansill Formation of the Permian Reef Complex, and are consistent with the Capitanian age of the Tansill reef. Samples at the center of the dike (youngest position) give $^{87}Sr/^{86}Sr$ near 0.7072 (Fig. 6). Without more work it is not possible

to know if the variation with position from the host is due to diagenesis or if it captures real changes in seawater through the growth of the cements. Rasbury et al. (2004) dated similar cements from the algal mounds of the Laborcita Formation in the Sacramento Mountains of New Mexico, and obtained ages and $^{87}Sr/^{86}Sr$ that were also consistent with the biostratigraphically constrained age of deposition.

Laser ablation maps of WC-1 are presented in Roberts et al. (2017). Sr concentrations range up to 7000 ppm, and regions with high Sr have high U. Magnesium is elevated in veins along with V and Mn, as is also shown with μXRF(Fig. 4) and TES (Fig. 7). While LA and μXRF do not offer the high resolution of synchrotron XRF, they do provide details at the scale that LA dating could be accomplished and few elements are inaccessible with quadrupole mass spectrometers.

High resolution, on the fly (the sample is continually moving and the detector is accumulating counts over a prescribed distance) element mapping in the tender energy range (TES) allows us to examine U, Mg, Sr and S in the Walnut Canyon sample. Comparing U, S, and Sr in a RGB map (Fig. 7) illustrates the spotty retention of Sr and S relative to U. As seen in the μXRF images (Fig. 4), Mg is elevated in veins and is thus introduced by later fluids. U(M5) XANES shows that the botryoidal cements have entirely oxidized U (Fig. 8). Uranium concentration in this sample is less than 5 ppm, and the ability to explore U oxidation states at this concentration is a major advance. An important factor to be considered for exploring for favorable U/Pb in carbonates is how U is incorporated. In the Walnut Canyon case we hypothesize the uranyl was brought to the site of precipitation by an oxidizing fluid (seawater) and structurally incorporated in aragonite which does not exclude U (Reeder et al., 2001; Kelly et al., 2003). Through neomorphism to calcite, U was left behind because active functional groups such as carboxyl have a high affinity for uranyl. Perhaps calcite grew around these complexed U ions preserving near original U concentrations. In contrast, Sr, which is also strongly partitioned into aragonite but has a lower affinity for calcite, was lost to the fluid because it does not have an affinity for organic matter.

2.2 Middle Miocene Tufa- Barstow Formation

The Middle Miocene Barstow Formation crops out in the Rainbow Basin near Barstow California. Tufa mounds are found near the top of the Owl Conglomerate (Cole et al., 2004, 2005) and are assumed to have formed where springs entered a lake similar to Mono and Pyramid Lake tufa towers. These tufa deposits have more than 100 ppm U, several ppm Pb and favorable U-Pb systematics (Cole et al., 2005). Here we build on the work of Cole et al. (2004, 2005) with additional synchrotron imaging, μXRF imaging and spectroscopy techniques. The sample that we are using to illustrate these tools for characterization is large enough to be suitable for distribution as a secondary reference material for LA carbonate dating (Fig. 9). Most of the samples used in the Cole et al. (2005) study were small slabs from Vicki Pedone (Cal State Northridge) and are too small to to distribute beyond our lab. Here, we are characterizing a new sample that is large enough to distribute widely. The previously studied tufa samples ranged in age from 14.8-17 Ma (Cole et al., 2005), so more work will be needed to determine the exact age of this sample.

Becker et al. (2001) showed that layers in the Barstow tufa deposits have a pattern of low (10ppm) to high (several hundred ppm) U concentrations across laminae revealed by fission track mapping. Uranium is lower at the base of laminae where larger crystals of calcite formed, and is higher in micritic calcite which forms the caps of laminae. Becker et al. (2001) reasoned that

the laminae reflect seasonal increases in fresh water supply which delivers Ca to a body of water with high alkalinity similar to the Great Basin Lakes. Phosphor imaging shows that in addition to these fine scale trends observed with fission tracks, there are mm to cm scale layers of higher and lower U concentrations (Cole et al., 2004).

Synchrotron and μXRF imaging of Sr and Mn faithfully matches the primary layering, demonstrating that later alteration has been minor (Fig. 10, Fig. 11). A comparison of U-L α maps with and without an incident radiation filter shows that the filter eliminates artifacts that result from scatter in pores, and returns an accurate map of the U (Fig. 12). The filtered U μXRF map shows that U is elevated in the micritic areas of the tufa. μXRF maps of Al and Si show that large pores that are typical of the tufa deposits have clay minerals lining them (Fig. 11). Fe, Cu and Zn are also elevated in the pores. A map of Ba closely matches the S map suggesting that barite may be present. Strontianite is found in economic abundance in the Barstow Formation (Knopf, 1917). The extremely high Sr concentrations in the tufa calcite (10's of thousands of ppm), suggests these fluids were contributing Sr during deposition. The $^{87}Sr/^{86}Sr$ isotope ratios of 3 aliquots ranged from 0.719877 to 0.721038 (Table 1). More work will be needed to determine if this sample can be a Sr isotope reference material as well as a secondary U/Pb carbonate reference material.

The U in these tufas is in the reduced state U^{4+} as shown by measurements at the L3 edge (Cole et al., 2004), and new data from the M5 edge (Fig. 13). With the high U concentration, the Barstow tufa could be a reference material for U XANES analyses. The Barstow tufa calcite is luminescent throughout (Fig. 14), consistent with the occurrence of reduced U in this sample. While it is easy to conceive of a stratified lake with reducing bottom waters, reduced U is insoluble in most solutions (Langmuir, 1978), begging the question of how it is available to go into the calcite. Elevated actinide concentrations are found in the Great Basin lakes, and it is thought that the carbonate alkalinity is responsible for this elevation (Anderson et al., 1982; Simpson et al., 1982). Similarly, Tullborg et al. (2017) demonstrates U(VI) complexes in extremely reducing fluids of deep groundwaters in Sweden. It seems clear that there is a kinetic barrier to U reduction even in the most reducing fluids, and yet some carbonates have entirely reduced U in their structures (Sturchio, 1998; Cole et al., 2004). More work is needed to understand the incorporation mechanism and use of synchrotron facilities to image the distribution of U with respect to other elements, and XAS measurements of U and other redox sensitive elements are important tools for advancing this research. Additionally lab directed studies that can produce U^{4+} in carbonates would be a huge leap forward.

One of the biggest advances in LAcarb dating is a contribution by Drost et al. (2018) which used laser ablation imaging and inspection for concentrations or ratios that reflect something that could be considered to be related (like Sr concentrations). Pooling of pixels based on this criteria from across the mapped region and binning based on some additional criteria like $^{235}U/^{207}Pb$ gives isochron plots with range of values that is typically greater than, and certainly more filled in than, would be obtained by spot analyses. The approach is justified because it would not be possible to select pixels based on criteria other than the ratios being plotted, that would have a meaningful isochron result if the assumption were invalid. This work built on a monocle approach introduced by Petrus et al. (2017) which provided a visual tool to easily compare maps, ratios, and patterns (such as REE patterns) that can be defined by the user. This package of tools is available in Iolite3 and Iolite4 and, beyond U-Pb dating, offers tremendous potential to better understand relationships between elements and how that relates to deposition and diagenesis. Inspired by the Drost et al. (2018) contribution, we did 45 laser ablation lines on the Barstow tufa

(Fig. 15). We used Iolite4 (Paton et al., 2011) for the data reduction. Note the laminae are easily visible in the element maps 15. While the U concentration is not as high in the sparry calcite layers, the U/Th and $^{238}U/^{206}Pb$ ratios are much higher than the micritic calcite 15. Similarly, the $^{208}Pb/^{206}Pb$ and $^{207}Pb/^{206}Pb$ are much lower, showing the radiogenic ingrowth of ^{206}Pb. Sr and Mg concentrations are elevated in the sparry calcite so μXRF maps of slabs would provide a framework for selection of spots for LAcarb (Fig. 11). We extracted pixels based on the criteria that they were greater than 12,500 ppm Sr. We used this value based on the monocle feature in Iolite4 which allowed us to see that this would eliminate most of the pixels outside the sparry calcite (Fig. 16). Nearly 7000 pixels meet the criteria for being greater than 12,500 ppm Sr and less than 1 ppm ^{208}Pb. These were subdivided into 90 bins of 70-80 pixels each based on probability of the $^{207}Pb/^{235}U$ ratio e.g. (Drost et al., 2018). When all of the bins are plotted on a Tera-Wasserburg concordia plot in Iosplot (Ludwig, 2003), there are tails on the low and high ends of the line. Removing 10% on each end produces a much better line (Fig. 16). The age of 11 Ma is about 20% too young. We did not make a correction because we do not know the age of this sample, but a correction could be made based on the secondary reference material and applied to unknowns. The purpose here is not to provide the age, but to show that the sample is very well behaved. Pre-screening with μXRF to establish the best regions to use for LAcarb should produce a reproducible secondary reference material for QA/QC.

2.3 Middle Miocene Dolomite

A Miocene conglomerate horizon in the Napenagila fossil locality of the Turkana Basin in Kenya is extensively cemented by calcite and dolomite. The dolomite is unique in a number of ways. It forms an isopachous layer on surfaces of fossil trees, showing that it formed in the saturated zone. It has a bladed habit, and is a bright yellow color, becoming darker yellow in the growth direction (Fig. 17). While only an outer crust of the sample has typical bright orange luminescence, the sample glows in the luminescope (Fig. 17). The dolomite has variable trace element concentrations along the growth direction, and extreme U enrichment in the final phases of growth as shown by synchrotron XRF element mapping (Fig. 18), μXRF (Fig. 19) and laser ablation (Fig. 20). The bladed morphology of the dolomite crystals is strongly emphasized by trace element patterns in the youngest part of the dolomite, and is particularly striking in the very high resolution maps from TES (Fig. 18). U M5 XANES shows that the U in the dolomite is in the reduced state (Fig. 22). The stratigraphic context of this dolomite and other carbonates from the Turkana Basin is being studied by Kevin Hatton and will be presented in a more comprehensive way elsewhere. Meanwhile, the very well-behaved U-Pb systematics make this a possible dolomite reference material, and the XRF mapping and X-ray spectroscopy make it a good example for carbonate characterization. The $^{238}U/^{206}Pb$ ratios for the dolomite sample range from 250-550. Using a selection criteria of U concentrations greater than 500, 600, 700 ppm, and ^{208}Pb less than 0.3 ppm produces over 1683, 1043, 452 pixels. Binning the pixels into 50,30,20 pixel bins produces data that form a small cluster that does not lead itself to the isochron approach. Plotted on the Wetherill type concordia plot, the data overlap with concordia and give a nominal age of an age of about 12 Ma (Fig. 21). Based on the Barstow results the age is likely slightly older. However, because this is a dolomite, more work is needed to understand how the different matrix will affect the U/Pb fractionation.

$^{87}Sr/^{86}Sr$ of three aliquots of the Turkana dolomite from the outside (oldest) to the inside (youngest) are indistinguishable from each other at 0.703306 (Table 2). With the well behaved U/Pb systematics, high concentrations of reduced U and homogeneous $^{87}Sr/^{86}Sr$, and further work in collaboration with other labs, this sample could be a reference material for U/Pb dating, Sr isotopes, and synchrotron U spectroscopy.

3 Summary

Field relationships and petrography allow us to consider the relative timing of carbonate precipitation and alteration, and the tools for demonstrating these relationships are an important first step to any study. XRF mapping (both μXRF and synchrotron XRF) and laser ablation mapping allows us to establish domains within rocks that are time-equivalent and to work out details of the fluids that were responsible for carbonate precipitation. Details such as the U oxidation state and relationships to other elements helps to further constrain the fluids that have produced the final product. While the U oxidation state does not appear to matter for the reliability of U-Pb ages, a general pattern of elevated U is emerging for samples with reduced U. While elevated U is not necessary for U-Pb dating, samples that are amenable to LA Carb dating typically must have ppm levels of U. The tools we have described here allow us to provide a spatial context that with well established petrography and field relationships are foundational for putting U-Pb ages into the overall geologic context.

Author contributions. ETR led the effort to review the literature on carbonate characterization. TP did the μXRF imaging of the carbonate standard materials. PN RT, and AL led the efforts for the synchrotron XRF and XANES measurements. KW and KH led the laser ablation mapping efforts. KW did the Sr isotope analyses. JMC did the work on the Barstow tufa. All of the authors contributed to writing the manuscript.

Competing interests. We declare that there are no competing interests.

Acknowledgements. Portions of this work were performed at beamline X26A of the National Synchrotron Light Source (NSLS), Brookhaven National Laboratory. X26A was supported by the Department of Energy (DOE) - Geosciences (DE-FG02-92ER14244 to The University of Chicago - CARS). Use of the NSLS was supported by DOE under Contract No. DE-AC02-98CH10886. Portions of this research were also performed at the Tender Energy Spectroscopy (TES), X-ray Fluorescence Microprobe (XFM), and Submicron Resolution X-ray Spectroscopy (SRX) beamlines and used resources of the National Synchrotron Light Source II, a U.S. Department of Energy (DOE) Office of Science User Facility operated for the DOE Office of Science by Brookhaven National Laboratory under Contract No. DE-SC0012704. Construction of, and work at the TES Beamline was partly funded by the National Science Foundation, Earth Sciences (EAR-1128957), NASA (NNX13AD12G) and the Department of Energy, Geosciences (DE-FG02-12ER16342). μXRF data was acquired in the Caltech GPS Division Analytical Facility with the support of Chi Ma, John Grotzinger, and the Simons Foundation. We thank Stephen Cox, Frank Sousa,

Elena Steponaitis and Sidney Hemming for the discovery of the dolomite in the Turkana Basin and acknowledge funding from the Columbia University Global Center for field work. Numerous discussions with Bruce Ward have greatly improved our understanding of carbonates. Journal reviewers Don Davis and an anonymous reviewer as well as associate editor Nick Roberts are thanked for their thoughtful comments which help improve the clarity of the manuscript.

References

Allwood, A. C., Rosing, M. T., Flannery, D. T., Hurowitz, J. A., and Heirwegh, C. M.: Reassessing evidence of life in 3,700-million-year-old rocks of Greenland, Nature, 563, 241–244, https://doi.org/10.1038/s41586-018-0610-4, http://www.nature.com/articles/s41586-018-0610-4, 2018.

Amiel, A. J., Miller, D. S., and Friedman, G. M.: Incorporation of uranium in modern corals, Sedimentology, 20, 523–528, https://doi.org/10.1111/j.1365-3091.1973.tb01629.x, http://doi.wiley.com/10.1111/j.1365-3091.1973.tb01629.x, 1973.

Anderson, R. F., Bacon, M. P., and Brewer, P. G.: Elevated Concentrations of Actinides in Mono Lake, Science, 216, 514–516, https://doi.org/10.1126/science.216.4545.514, https://www.sciencemag.org/lookup/doi/10.1126/science.216.4545.514, 1982.

Banner, J. L. and Hanson, G. N.: Calculation of simultaneous isotopic and trace element variations during water-rock interaction with applications to carbonate diagenesis, Geochimica et Cosmochimica Acta, 54, 3123–3137, https://doi.org/10.1016/0016-7037(90)90128-8, https://linkinghub.elsevier.com/retrieve/pii/0016703790901288, 1990.

Barnaby, R. and Rimstidt, J.: Redox conditions of calcite cementation interpreted from Mn-contents and Fe-contents of authigenic calcites, Geological Society of America Bulletin, 101, 795–804, https://doi.org/10.1130/0016-7606(1989)101<0795:RCOCCI>2.3.CO;2, 1989.

Becker, M., Cole, J., Rasbury, E., Pedone, V., Montanez, I., and Hanson, G.: Cyclic variations of uranium concentrations and oxygen isotopes in tufa from the middle Miocene Barstow Formation, Mojave Desert, California, GEOLOGY, 29, 139–142, https://doi.org/10.1130/0091-7613(2001)029<0139:CVOUCA>2.0.CO;2, 2001.

Becker, M., Rasbury, E., Meyers, W., and Hanson, G.: U–Pb calcite age of the Late Permian Castile Formation, Delaware Basin: a constraint on the age of the Permian–Triassic boundary (?), Earth and Planetary Science Letters, 203, 681–689, https://doi.org/10.1016/S0012-821X(02)00877-4, https://linkinghub.elsevier.com/retrieve/pii/S0012821X02008774, 2002.

Bishop, J. W., Osleger, D. A., Montañez, I. P., and Sumner, D. Y.: Meteoric diagenesis and fluid-rock interaction in the Middle Permian Capitan backreef: Yates Formation, Slaughter Canyon, New Mexico, AAPG Bulletin, 98, 1495–1519, https://doi.org/10.1306/05201311158, http://search.datapages.com/data/doi/10.1306/05201311158, 2014.

Brannon, J. C., Cole, S. C., Podosek, F. A., Ragan, V. M., Coveney, R. M., Wallace, M. W., and Bradley, A. J.: Th-Pb and U-Pb Dating of Ore-Stage Calcite and Paleozoic Fluid Flow, Science, 271, 491–493, https://doi.org/10.1126/science.271.5248.491, https://www.sciencemag.org/lookup/doi/10.1126/science.271.5248.491, 1996.

Budd, D. A., Frost, E. L., Huntington, K. W., and Allwardt, P. F.: Syndepositional Deformation Features In High-Relief Carbonate Platforms: Long-Lived Conduits for Diagenetic Fluids, Journal of Sedimentary Research, 83, 12–36, https://doi.org/10.2110/jsr.2013.3, https://pubs.geoscienceworld.org/jsedres/article/83/1/12-36/145369, 2013.

Chafetz, H. S., Wu, Z., Lapen, T. J., and Milliken, K. L.: Geochemistry of Preserved Permian Aragonitic Cements in the Tepees of the Guadalupe Mountains, West Texas and New Mexico, U.S.A., Journal of Sedimentary Research, 78, 187–198, https://doi.org/10.2110/jsr.2008.025, https://pubs.geoscienceworld.org/jsedres/article/78/3/187-198/145192, 2008.

Chung, G. and Swart, P.: The concentration of uranium in fresh-water vadose and phreatic cements in a Holocene ooid cay- A method of identifying ancient water tables, Journal of Sedimentary Petrology, 60, 735–746, 1990.

Cole, J. M., Nienstedt, J., Spataro, G., Rasbury, E., Lanzirotti, A., Celestian, A. J., Nilsson, M., and Hanson, G. N.: Phosphor imaging as a tool for in situ mapping of ppm levels of uranium and thorium in rocks and minerals, Chemical Geology, 193, 127–136, https://doi.org/10.1016/S0009-2541(02)00223-1, https://linkinghub.elsevier.com/retrieve/pii/S0009254102002231, 2003.

Cole, J. M., Rasbury, E. T., Montañez, I. P., Pedone, V. A., Lanzirotti, A., and Hanson, G. N.: Petrographic and trace element analysis of uranium-rich tufa calcite, middle Miocene Barstow Formation, California, USA: Uranium-rich tufa deposits, California, Sedimentology, 51, 433–453, https://doi.org/10.1111/j.1365-3091.2004.00631.x, http://doi.wiley.com/10.1111/j.1365-3091.2004.00631.x, 2004.

Cole, J. M., Rasbury, E. T., Hanson, G. N., Montañez, I. P., and Pedone, V. A.: Using U-Pb ages of Miocene tufa for correlation in a terrestrial succession, Barstow Formation, California, Geological Society of America Bulletin, 117, 276, https://doi.org/10.1130/B25553.1, https://pubs.geoscienceworld.org/gsabulletin/article/117/3-4/276-287/2146, 2005.

de Winter, N. J. and Claeys, P.: Micro X-ray fluorescence (XRF) line scanning on Cretaceous rudist bivalves: A new method for reproducible trace element profiles in bivalve calcite, SEDIMENTOLOGY, 64, 231–251, https://doi.org/10.1111/sed.12299, 2017.

de Winter, N. J., Sinnesael, M., Makarona, C., Vansteenberge, S., and Claeys, P.: Trace element analyses of carbonates using portable and micro-X-ray fluorescence: performance and optimization of measurement parameters and strategies, Journal of Analytical Atomic Spectrometry, 32, 1211–1223, https://doi.org/10.1039/C6JA00361C, http://xlink.rsc.org/?DOI=C6JA00361C, 2017.

Dickson, J. A. D. and Kenter, J. A. M.: Diagenetic Evolution of Selected Parasequences Across A Carbonate Platform: Late Paleozoic, Tengiz Reservoir, Kazakhstan, Journal of Sedimentary Research, 84, 664–693, https://doi.org/10.2110/jsr.2014.54, https://pubs.geoscienceworld.org/jsedres/article/84/8/664-693/145419, 2014.

Drake, H., Mathurin, F. A., Zack, T., Schaefer, T., Roberts, N. M. W., Whitehouse, M., Karlsson, A., Broman, C., and Astrom, M. E.: Incorporation of Metals into Calcite in a Deep Anoxic Granite Aquifer, ENVIRONMENTAL SCIENCE & TECHNOLOGY, 52, 493–502, https://doi.org/10.1021/acs.est.7b05258, 2018.

Drost, K., Chew, D., Petrus, J. A., Scholze, F., Woodhead, J. D., Schneider, J. W., and Harper, D. A. T.: An Image Mapping Approach to U-Pb LA-ICP-MS Carbonate Dating and Applications to Direct Dating of Carbonate Sedimentation, Geochemistry, Geophysics, Geosystems, 19, 4631–4648, https://doi.org/10.1029/2018GC007850, http://doi.wiley.com/10.1029/2018GC007850, 2018.

Drysdale, R. N., Zanchetta, G., Baneschi, I., Guidi, M., Isola, I., Couchoud, I., Piccini, L., Greig, A., Wong, H., Woodhead, J. D., Regattieri, E., Corrick, E., Paul, B., Spötl, C., Denson, E., Gordon, J., Jaillet, S., Dux, F., and Hellstrom, J. C.: Partitioning of Mg, Sr, Ba and U into a subaqueous calcite speleothem, Geochimica et Cosmochimica Acta, 264, 67–91, https://doi.org/10.1016/j.gca.2019.08.001, https://linkinghub.elsevier.com/retrieve/pii/S0016703719304995, 2019.

Frisia, S., Borsato, A., and Susini, J.: Synchrotron radiation applications to past volcanism archived in speleothems: An overview, Journal of Volcanology and Geothermal Research, 177, 96–100, https://doi.org/10.1016/j.jvolgeores.2007.11.010, https://linkinghub.elsevier.com/retrieve/pii/S0377027307003794, 2008.

Frost, E. L., Budd, D. A., and Kerans, C.: Syndepositional Deformation In A High-Relief Carbonate Platform and Its Effect On Early Fluid Flow As Revealed By Dolomite Patterns, Journal of Sedimentary Research, 82, 913–932, https://doi.org/10.2110/jsr.2012.74, https://pubs.geoscienceworld.org/jsedres/article/82/12/913-932/245332, 2013.

Godeau, N., Deschamps, P., Guihou, A., Leonide, P., Tendil, A., Gerdes, A., Hamelin, B., and Girard, J.-P.: U-Pb dating of calcite cement and diagenetic history in microporous carbonate reservoirs: Case of the Urgonian Limestone, France, Geology, 46, 247–250, https://doi.org/10.1130/G39905.1, https://pubs.geoscienceworld.org/gsa/geology/article/46/3/247/526712/UPb-dating-of-calcite-cement-and-diagenetic, 2018.

Grotzinger, J. P. and Knoll, A. H.: Anomalous Carbonate Precipitates: Is the Precambrian the Key to the Permian?, PALAIOS, 10, 578, https://doi.org/10.2307/3515096, https://pubs.geoscienceworld.org/palaios/article/10/6/578-596/114257, 1995.

Gvirtzman, G., Friedman, G., and Miller, D.: Conntrol and distribution of uranium in coral reefs during diagenesis, Journal of Sedimentary Petrology, 43, 985–997, 1973.

Haglund, D., Friedman, G., and Miller, D.: Effect of fresh water redistribution of uranium in carbonate sediments, Journal of Sedimentary Petrology, 39, 1283–&, 1969.

Hardie, L.: Secular variation in seawater chemistry: An explanation for the coupled secular variation in the mineralogies of marine limestones and potash evaporites over the past 600 my, Geology, 24, 279–283, https://doi.org/10.1130/0091-7613(1996)024<0279:SVISCA>2.3.CO;2, 1996.

Hoff, J., Jameson, J., and Hanson, G.: Application of Pb isotopes to the absolute timing of regional exposure events in carbonate rocks- an example from U-rich dolostones from the Wahoo Formation (Pennsylvanian), Prudhoe Bay, Alaska A, Journal of Sedimentary Research Section A -Sedimentary Petrology and Processes, 65, 225–233, 1995.

Horita, J., Zimmermann, H., and Holland, H. D.: Chemical evolution of seawater during the Phanerozoic, Geochimica et Cosmochimica Acta, 66, 3733–3756, https://doi.org/10.1016/S0016-7037(01)00884-5, https://linkinghub.elsevier.com/retrieve/pii/S0016703701008845, 2002.

Hunt, D. W., Fitchen, W. M., and Kosa, E.: Syndepositional deformation of the Permian Capitan reef carbonate platform, Guadalupe Mountains, New Mexico, USA, Sedimentary Geology, 154, 89–126, https://doi.org/10.1016/S0037-0738(02)00104-5, https://linkinghub.elsevier.com/retrieve/pii/S0037073802001045, 2003.

Jones, C., Halliday, A., and Lohmann, K.: The impact of diagenesis on high-precision UPb dating of ancient carbonates: An example from the Late Permian of New Mexico, Earth and Planetary Science Letters, 134, 409–423, https://doi.org/10.1016/0012-821X(95)00128-Y, https://linkinghub.elsevier.com/retrieve/pii/0012821X9500128Y, 1995.

Katsuta, N., Takano, M., Sano, N., Tani, Y., Ochiai, S., Naito, S., Murakami, T., Niwa, M., and Kawakami, S.: Quantitative micro-X-ray fluorescence scanning spectroscopy of wet sediment based on the X-ray absorption and emission theories: Its application to freshwater lake sedimentary sequences, Sedimentology, 66, 2490–2510, https://doi.org/10.1111/sed.12603, https://onlinelibrary.wiley.com/doi/abs/10.1111/sed.12603, 2019.

Kelly, S. D., Newville, M. G., Cheng, L., Kemner, K. M., Sutton, S. R., Fenter, P., Sturchio, N. C., and Spötl, C.: Uranyl Incorporation in Natural Calcite, Environmental Science & Technology, 37, 1284–1287, https://doi.org/10.1021/es025962f, https://pubs.acs.org/doi/10.1021/es025962f, 2003.

Kelly, S. D., Rasbury, E. T., Chattopadhyay, S., Kropf, A. J., and Kemner, K. M.: Evidence of a Stable Uranyl Site in Ancient Organic-Rich Calcite, Environmental Science & Technology, 40, 2262–2268, https://doi.org/10.1021/es051970v, https://pubs.acs.org/doi/10.1021/es051970v, 2006.

Knopf, A.: Strontianite deposits near Barstow California, Tech. rep., 1917.

Langmuir, D.: Uranium solution-mineral equilibria at low-temperatures with applications to sedimentary ore-deposits U, Geochimica et Cosmochimica Acta, 42, 547–569, https://doi.org/10.1016/0016-7037(78)90001-7, 1978.

Lawson, M., Shenton, B. J., Stolper, D. A., Eiler, J. M., Rasbury, E. T., Becker, T. P., Phillips-Lander, C. M., Buono, A. S., Becker, S. P., Pottorf, R., Gray, G. G., Yurewicz, D., and Gournay, J.: Deciphering the diagenetic history of the El Abra Formation of eastern Mexico using reordered clumped isotope temperatures and U-Pb dating, GEOLOGICAL SOCIETY OF AMERICA BULLETIN, 130, 617–629, https://doi.org/10.1130/B31656.1, 2018.

Lowenstein, T. K.: Oscillations in Phanerozoic Seawater Chemistry: Evidence from Fluid Inclusions, Science, 294, 1086–1088, https://doi.org/10.1126/science.1064280, https://www.sciencemag.org/lookup/doi/10.1126/science.1064280, 2001.

Loyd, S., Dickson, J., Scholle, P., and Tripati, A.: Extensive, uplift-related and non-fault-controlled spar precipitation in the Permian Capitan Formation, Sedimentary Geology, 298, 17–27, https://doi.org/10.1016/j.sedgeo.2013.10.001, https://linkinghub.elsevier.com/retrieve/pii/S0037073813001887, 2013.

Luczaj, J. A. and Goldstein, R. H.: Diagenesis of the Lower Permian Krider Member, Southwest Kansas, U.S.A.: Fluid-Inclusion, U-Pb, and Fission-Track Evidence for Reflux Dolomitization During Latest Permian Time, Journal of Sedimentary Research, 70, 762–773, https://doi.org/10.1306/2DC40936-0E47-11D7-8643000102C1865D, https://pubs.geoscienceworld.org/jsedres/article/70/3/762-773/99155, 2000.

Ludwig, K.: Uranium-daughter migration and U-Pb isotope apparent ages of uranium ores, Shirley Basin, Wyoming, Economic Geology, 73, 29–49, https://doi.org/10.2113/gsecongeo.73.1.29, 1978.

Ludwig, K. R.: ISOPLOT 3.0: a geochronological toolkit for Microsoft Excel Volume: 4, 2003.

Meyers, W.: Carbonate cement stratigraphy of the Lake Valley Formation (Mississippian) Sacramento Mountains, New Mexico, Journal of Sedimentary Petrology, 44, 837–861, 1974.

Meyers, W.: Calcite cement stratigraphy- An overview, in: Luminescence microscopy and spectroscopy: Qualitative and quantitative applications, edited by BARKER, CE and KOPP, OC, vol. 25 of *SEPM Short coure notes*, pp. 133–148, Society Sedimentary Geology, 1991.

Migdisov, A., Guo, X., Williams-Jones, A., Sun, C., Vasyukova, O., Sugiyama, I., Fuchs, S., Pearce, K., and Roback, R.: Hydrocarbons as ore fluids, Geochemical Perspectives Letters, pp. 47–52, https://doi.org/10.7185/geochemlet.1745, http://www.geochemicalperspectivesletters.org/article1745, 2017.

Musgrove, M. and Banner, J. L.: Regional Ground-Water Mixing and the Origin of Saline Fluids: Midcontinent, United States, Science, 259, 1877–1882, https://doi.org/10.1126/science.259.5103.1877, https://www.sciencemag.org/lookup/doi/10.1126/science.259.5103.1877, 1993.

Northrup, P.: The TES beamline (8-BM) at NSLS-II: tender-energy spatially resolved X-ray absorption spectroscopy and X-ray fluorescence imaging, Journal of Synchrotron Radiation, 26, 2064–2074, https://doi.org/10.1107/S1600577519012761, http://scripts.iucr.org/cgi-bin/paper?S1600577519012761, 2019.

Ortega, R., Devès, G., and Maire, R.: Nuclear microprobe analysis of uranium-rich speleothems: Methodological aspects, Nuclear Instruments and Methods in Physics Research Section B: Beam Interactions with Materials and Atoms, 210, 455–458, https://doi.org/10.1016/S0168-583X(03)01075-9, https://linkinghub.elsevier.com/retrieve/pii/S0168583X03010759, 2003.

Ortega, R., Maire, R., Devès, G., and Quinif, Y.: High-resolution mapping of uranium and other trace elements in recrystallized aragonite–calcite speleothems from caves in the Pyrenees (France): Implication for U-series dating, Earth and Planetary Science Letters, 237, 911–923, https://doi.org/10.1016/j.epsl.2005.06.045, https://linkinghub.elsevier.com/retrieve/pii/S0012821X05004243, 2005.

Pagel, M., Bonifacie, M., Schneider, D. A., Gautheron, C., Brigaud, B., Calmels, D., Cros, A., Saint-Bezar, B., Landrein, P., Sutcliffe, C., Davis, D., and Chaduteau, C.: Improving paleohydrological and diagenetic reconstructions in calcite veins and breccia of a sedimentary basin by combining $\Delta 47$ temperature, 18Owater and U-Pb age, Chemical Geology, 481, 1–17, https://doi.org/10.1016/j.chemgeo.2017.12.026, https://linkinghub.elsevier.com/retrieve/pii/S0009254117307076, 2018.

Parrish, J. T., Rasbury, E. T., Chan, M. A., and Hasiotis, S. T.: Earliest Jurassic U-Pb ages from carbonate deposits in the Navajo Sandstone, southeastern Utah, USA, Geology, 47, 1015–1019, https://doi.org/10.1130/G46338.1, https://pubs.geoscienceworld.org/gsa/geology/article/47/11/1015/573442/Earliest-Jurassic-UPb-ages-from-carbonate-deposits, 2019.

Paton, C., Hellstrom, J., Paul, B., Woodhead, J., and Hergt, J.: Iolite: Freeware for the visualisation and processing of mass spectrometric data, Journal of Analytical Atomic Spectrometry, 26, 2508, https://doi.org/10.1039/c1ja10172b, http://xlink.rsc.org/?DOI=c1ja10172b, 2011.

Petrus, J. A., Chew, D. M., Leybourne, M. I., and Kamber, B. S.: A new approach to laser-ablation inductively-coupled-plasma mass spectrometry (LA-ICP-MS) using the flexible map interrogation tool 'Monocle', CHEMICAL GEOLOGY, 463, 76–93, https://doi.org/10.1016/j.chemgeo.2017.04.027, 2017.

Piccione, G., Rasbury, E. T., Elliott, B. A., Kyle, J. R., Jaret, S. J., Acerbo, A. S., Lanzirotti, A., Northrup, P., Wooton, K., and Parrish, R. R.: Vein fluorite U-Pb dating demonstrates post–6.2 Ma rare-earth element mobilization associated with Rio Grande rifting, Geosphere, 15, 1958–1972, https://doi.org/10.1130/GES02139.1, https://pubs.geoscienceworld.org/gsa/geosphere/article/15/6/1958/574972/Vein-fluorite-UPb-dating-demonstrates-post62-Ma, 2019.

Pickering, R., Kramers, J. D., Hancox, P. J., de Ruiter, D. J., and Woodhead, J. D.: Contemporary flowstone development links early hominin bearing cave deposits in South Africa, Earth and Planetary Science Letters, 306, 23–32, https://doi.org/10.1016/j.epsl.2011.03.019, https://linkinghub.elsevier.com/retrieve/pii/S0012821X11001634, 2011.

Pisapia, C., Deschamps, P., Battani, A., Buschaert, S., Guihou, A., Hamelin, B., and Brulhet, J.: U/Pb dating of geodic calcite: new insights on Western Europe major tectonic events and associated diagenetic fluids, Journal of the Geological Society, 175, 60–70, https://doi.org/10.1144/jgs2017-067, http://jgs.lyellcollection.org/lookup/doi/10.1144/jgs2017-067, 2018.

Polyak, V., Hill, C., and Asmerom, Y.: Age and Evolution of the Grand Canyon Revealed by U-Pb Dating of Water Table-Type Speleothems, Science, 319, 1377–1380, https://doi.org/10.1126/science.1151248, https://www.sciencemag.org/lookup/doi/10.1126/science.1151248, 2008.

Polyak, V., DuChene, H., Davis, D., Palmer, A., Palmer, M., and Asmerom, Y.: Incision history of Glenwood Canyon, Colorado, USA, from the uranium-series analyses of water-table speleothems, International Journal of Speleology, 42, 193–202, https://doi.org/10.5038/1827-806X.42.3.3, http://scholarcommons.usf.edu/ijs/vol42/iss3/3/, 2013.

Quade, J., Rasbury, E., Huntington, K., Hudson, A., Vonhof, H., Anchukaitis, K., Betancourt, J., Latorre, C., and Pepper, M.: Isotopic characterization of late Neogene travertine deposits at Barrancas Blancas in the eastern Atacama Desert, Chile, Chemical Geology, 466, 41–56, https://doi.org/10.1016/j.chemgeo.2017.05.004, https://linkinghub.elsevier.com/retrieve/pii/S000925411730270X, 2017.

Rasbury, E., Hanson, G., Meyers, W., and Saller, A.: Dating of the time of sedimentation using UPb ages for paleosol calcite, Geochimica et Cosmochimica Acta, 61, 1525–1529, https://doi.org/10.1016/S0016-7037(97)00043-4, https://linkinghub.elsevier.com/retrieve/pii/S0016703797000434, 1997.

Rasbury, E., Ward, W., Hemming, N., Li, H., Dickson, J., Hanson, G., and Major, R.: Concurrent U–Pb age and seawater 87Sr/86Sr value of a marine cement, Earth and Planetary Science Letters, 221, 355–371, https://doi.org/10.1016/S0012-821X(04)00105-0, https://linkinghub.elsevier.com/retrieve/pii/S0012821X04001050, 2004.

Rasbury, E. T. and Cole, J. M.: Directly dating geologic events: U-Pb dating of carbonates, Reviews of Geophysics, 47, RG3001, https://doi.org/10.1029/2007RG000246, http://doi.wiley.com/10.1029/2007RG000246, 2009.

Rasbury, E. T., Meyers, W. J., Hanson, G. N., Goldstein, R. H., and Saller, A. H.: Relationship of Uranium to Petrography of Caliche Paleosols with Application to Precisely Dating the Time of Sedimentation, Journal of Sedimentary Research, 70, 604–618, https://doi.org/10.1306/2DC4092B-0E47-11D7-8643000102C1865D, https://pubs.geoscienceworld.org/jsedres/article/70/3/604-618/99126, 2000.

Reeder, R. J., Nugent, M., Tait, C., Morris, D. E., Heald, S. M., Beck, K. M., Hess, W. P., and Lanzirotti, A.: Coprecipitation of Uranium(VI) with Calcite: XAFS, micro-XAS, and luminescence characterization, Geochimica et Cosmochimica Acta, 65, 3491–3503, https://doi.org/10.1016/S0016-7037(01)00647-0, https://linkinghub.elsevier.com/retrieve/pii/S0016703701006470, 2001.

Roberts, N. M. W., Rasbury, E. T., Parrish, R. R., Smith, C. J., Horstwood, M. S. A., and Condon, D. J.: A calcite reference material for LA-ICP-MS U-Pb geochronology: Calcite RM for LA-ICP-MS U-Pb dating, Geochemistry, Geophysics, Geosystems, 18, 2807–2814, https://doi.org/10.1002/2016GC006784, http://doi.wiley.com/10.1002/2016GC006784, 2017.

Roberts, N. M. W., Drost, K., Horstwood, M. S. A., Condon, D. J., Chew, D., Drake, H., Milodowski, A. E., McLean, N. M., Smye, A. J., Walker, R. J., Haslam, R., Hodson, K., Imber, J., Beaudoin, N., and Lee, J. K.: Laser ablation inductively coupled plasma mass spectrometry (LA-ICP-MS) U–Pb carbonate geochronology: strategies, progress, and limitations, Geochronology, 2, 33–61, https://doi.org/10.5194/gchron-2-33-2020, https://gchron.copernicus.org/articles/2/33/2020/, 2020.

Runnells, D.: Diagenesis, chemical sediments, and mixing of natural waters, Journal of Sedimentary Petrology, 39, 1188–&, 1969.

S. J. Mazzullo: Calcite Pseudospar Replacive of Marine Acicular Aragonite, and Implications for Aragonite Cement Diagenesis, SEPM Journal of Sedimentary Research, Vol. 50, https://doi.org/10.1306/212F7A18-2B24-11D7-8648000102C1865D, https://pubs.geoscienceworld.org/jsedres/article/50/2/409-422/97298, 1980.

Scholle, P. A., Ulmer, D. S., and Melim, L. A.: Late-stage calcites in the Permian Capitan Formation and its equivalents, Delaware Basin margin, west Texas and New Mexico: evidence for replacement of precursor evaporites, Sedimentology, 39, 207–234, https://doi.org/10.1111/j.1365-3091.1992.tb01035.x, http://doi.wiley.com/10.1111/j.1365-3091.1992.tb01035.x, 1992.

Shen, G. T. and Boyle, E. A.: Determination of lead, cadmium and other trace metals in annually-banded corals, Chemical Geology, 67, 47–62, https://doi.org/10.1016/0009-2541(88)90005-8, https://linkinghub.elsevier.com/retrieve/pii/0009254188900058, 1988.

Simpson, H. J., Trier, R. M., Toggweiler, J. R., Mathieu, G., Deck, B. L., Olsen, C. R., Hammond, D. E., Fuller, C., and Ku, T. L.: Radionuclides in Mono Lake, California, Science, 216, 512–514, https://doi.org/10.1126/science.216.4545.512, https://www.sciencemag.org/lookup/doi/10.1126/science.216.4545.512, 1982.

Sturchio, N. C.: Tetravalent Uranium in Calcite, Science, 281, 971–973, https://doi.org/10.1126/science.281.5379.971, https://www.sciencemag.org/lookup/doi/10.1126/science.281.5379.971, 1998.

Sutton, S. R., Bertsch, P. M., Newville, M., Rivers, M., Lanzirotti, A., and Eng, P.: Microfluorescence and Microtomography Analyses of Heterogeneous Earth and Environmental Materials, Reviews in Mineralogy and Geochemistry, 49, 429–483, https://doi.org/10.2138/rmg.2002.49.8, https://pubs.geoscienceworld.org/rimg/article/49/1/429-483/140753, 2002.

Suzuki, Y., Mukai, H., Ishimura, T., Yokoyama, T. D., Sakata, S., Hirata, T., Iwatsuki, T., and Mizuno, T.: Formation and Geological Sequestration of Uranium Nanoparticles in Deep Granitic Aquifer, Scientific Reports, 6, https://doi.org/10.1038/srep22701, 2016.

Timofeev, A., Migdisov, A. A., Williams-Jones, A. E., Roback, R., Nelson, A. T., and Xu, H.: Uranium transport in acidic brines under reducing conditions, Nature Communications, 9, 1469, https://doi.org/10.1038/s41467-018-03564-7, http://www.nature.com/articles/s41467-018-03564-7, 2018.

Tullborg, E.-L., Suksi, J., Geipel, G., Krall, L., Auqué, L., Gimeno, M., and Puigdomenech, I.: The Occurrences of Ca2UO2(CO3)3 Complex in Fe(II) Containing Deep Groundwater at Forsmark, Eastern Sweden, Procedia Earth and Planetary Science, 17, 440–443, https://doi.org/10.1016/j.proeps.2016.12.111, https://linkinghub.elsevier.com/retrieve/pii/S187852201630145X, 2017.

Vanghi, V., Borsato, A., Frisia, S., Howard, D. L., Gloy, G., Hellstrom, J., and Bajo, P.: High-resolution synchrotron X-ray fluorescence investigation of calcite coralloid speleothems: Elemental incorporation and their potential as environmental archives, Sedimentology, 66, 2661–2685, https://doi.org/10.1111/sed.12607, https://onlinelibrary.wiley.com/doi/abs/10.1111/sed.12607, 2019.

Vermeesch, P.: IsoplotR: A free and open toolbox for geochronology, Geoscience Frontiers, 9, 1479–1493, https://doi.org/10.1016/j.gsf.2018.04.001, https://linkinghub.elsevier.com/retrieve/pii/S1674987118300835, 2018.

Wang, Z., Rasbury, E., Hanson, G., and Meyers, W.: Using the U-Pb system of calcretes to date the time of sedimentation of clastic sedimentary rocks, Geochimica et Cosmochimica Acta, 62, 2823–2835, https://doi.org/10.1016/S0016-7037(98)00201-4, https://linkinghub.elsevier.com/retrieve/pii/S0016703798002014, 1998.

Weremeichik, J. M., Gabitov, R. I., Thien, B. M., and Sadekov, A.: The effect of growth rate on uranium partitioning between individual calcite crystals and fluid, Chemical Geology, 450, 145–153, https://doi.org/10.1016/j.chemgeo.2016.12.026, https://linkinghub.elsevier.com/retrieve/pii/S0009254116306866, 2017.

Wigley, T. and Plummer, L.: Mixing of carbonate waters, Geochimica et Cosmochimica Acta, 40, 989–995, https://doi.org/10.1016/0016-7037(76)90041-7, 1976.

Williford, K. H., Farley, K. A., Stack, K. M., Allwood, A. C., Beaty, D., Beegle, L. W., Bhartia, R., Brown, A. J., de la Torre Juarez, M., Hamran, S.-E., Hecht, M. H., Hurowitz, J. A., Rodriguez-Manfredi, J. A., Maurice, S., Milkovich, S., and Wiens, R. C.: The NASA Mars 2020 Rover Mission and the Search for Extraterrestrial Life, in: From Habitability to Life on Mars, pp. 275–308, Elsevier, https://doi.org/10.1016/B978-0-12-809935-3.00010-4, https://linkinghub.elsevier.com/retrieve/pii/B9780128099353000104, 2018.

Winter, B. L. and Johnson, C. M.: UPb dating of a carbonate subaerial exposure event, Earth and Planetary Science Letters, 131, 177–187, https://doi.org/10.1016/0012-821X(95)00026-9, https://linkinghub.elsevier.com/retrieve/pii/0012821X95000269, 1995.

Woodhead, J., Reisz, R., Fox, D., Drysdale, R., Hellstrom, J., Maas, R., Cheng, H., and Edwards, R. L.: Speleothem climate records from deep time? Exploring the potential with an example from the Permian, Geology, 38, 455–458, https://doi.org/10.1130/G30354.1, http://pubs.geoscienceworld.org/geology/article/38/5/455/130254/Speleothem-climate-records-from-deep-time, 2010.

Woodhead, J. D., Hellstrom, J., Hergt, J. M., Greig, A., and Maas, R.: Isotopic and elemental imaging of geological materials by laser ablation inductively coupled plasma-mass spectrometry, Geostandards and Geoanalytical Research, 31, 331–343, 2007.

Wu, Q., Ramezani, J., Zhang, H., Yuan, D.-x., Erwin, D. H., Henderson, C. M., Lambert, L. L., Zhang, Y.-c., and Shen, S.-z.: High-precision U-Pb zircon age constraints on the Guadalupian in West Texas, USA, Palaeogeography, Palaeoclimatology, Palaeoecology, 548, 109 668, https://doi.org/10.1016/j.palaeo.2020.109668, https://linkinghub.elsevier.com/retrieve/pii/S0031018220301139, 2020.

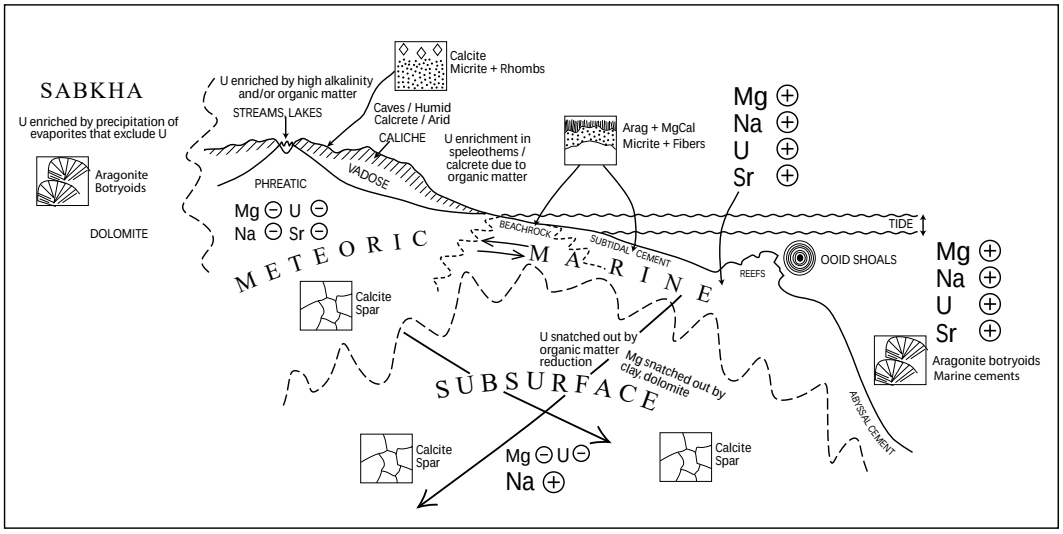

Figure 1. Cartoon of the variety of carbonate producing environments with arrows indicating the direction the elements would change through diagenetic alteration (Rasbury and Cole, 2009) We would like to see U concentrations and oxidation states be an important component in understanding fluids and diagenesis

.

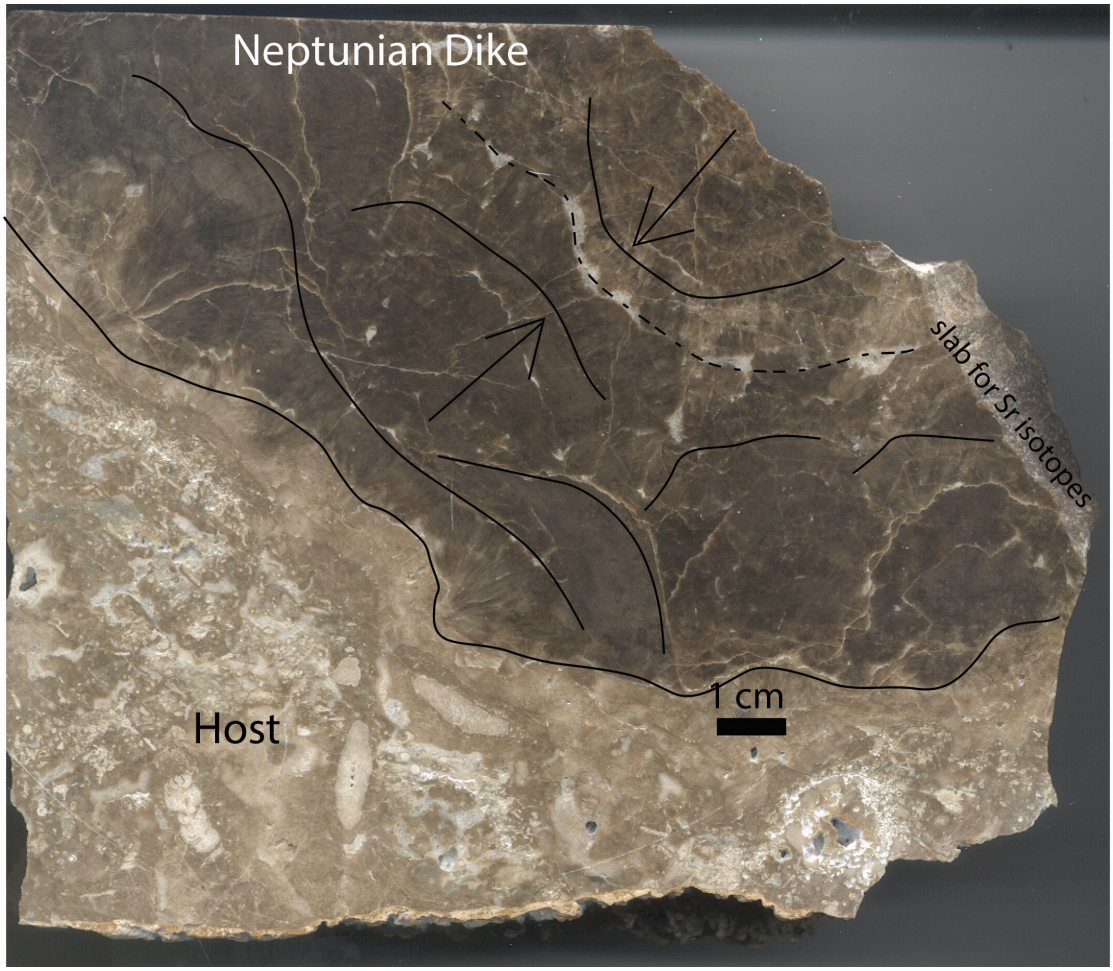

Figure 2. Large hand sample from a Neptunian dike at Walnut Canyon. The lighter brown limestone on the left is the reef rock with abundant large forams visible here. The dark brown botryoids can be seen growing from both sides of this oblique slab through the dike carbonate. Curved lines show approximate botryoid boundaries and arrows point in the growth direction. The dashed line is approximately the center of the dike. A white calcite cement lines many of the botryoids and occurs in the center of the dike. A slab from the host to the center was analyzed for the Sr isotopes presented in this paper.

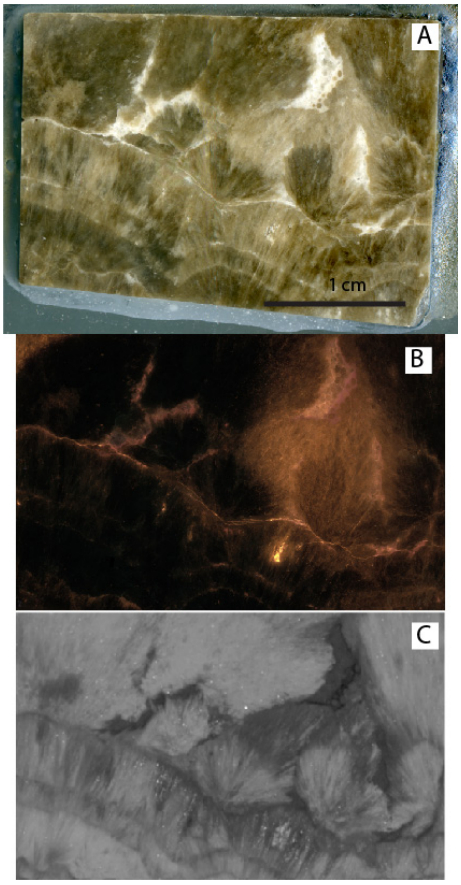

Figure 3. A. Polished slab from the Walnut Canyon Neptunian Dike sample used in this study to illustrate various tools for characterization. This is approximately 3 cm across. This is a similar size to that being distributed as a reference material (Roberts et al., 2017). Note the variability of color from very dark to light brown, and white veins. The fibrous botyroidal texture is visible even at this scale, and complexities due to veins should be easily avoided when using this as a LAcarb reference material. B. Photomosaic of 639 CL photos. C. MicroXRF map of Sr (details in the next figure caption). Areas that are brightly luminescent have low Sr. Boundaries between botryoid layers are luminescent (and white so easy to avoid) and should be avoided when using this sample as a standard. This microXRF map of Sr beautifully shows the texture of the sample. We suggest that this easy screening technique could be done on all slabs being used for a LA standard, and that this could result in better reproducibility of measurements.

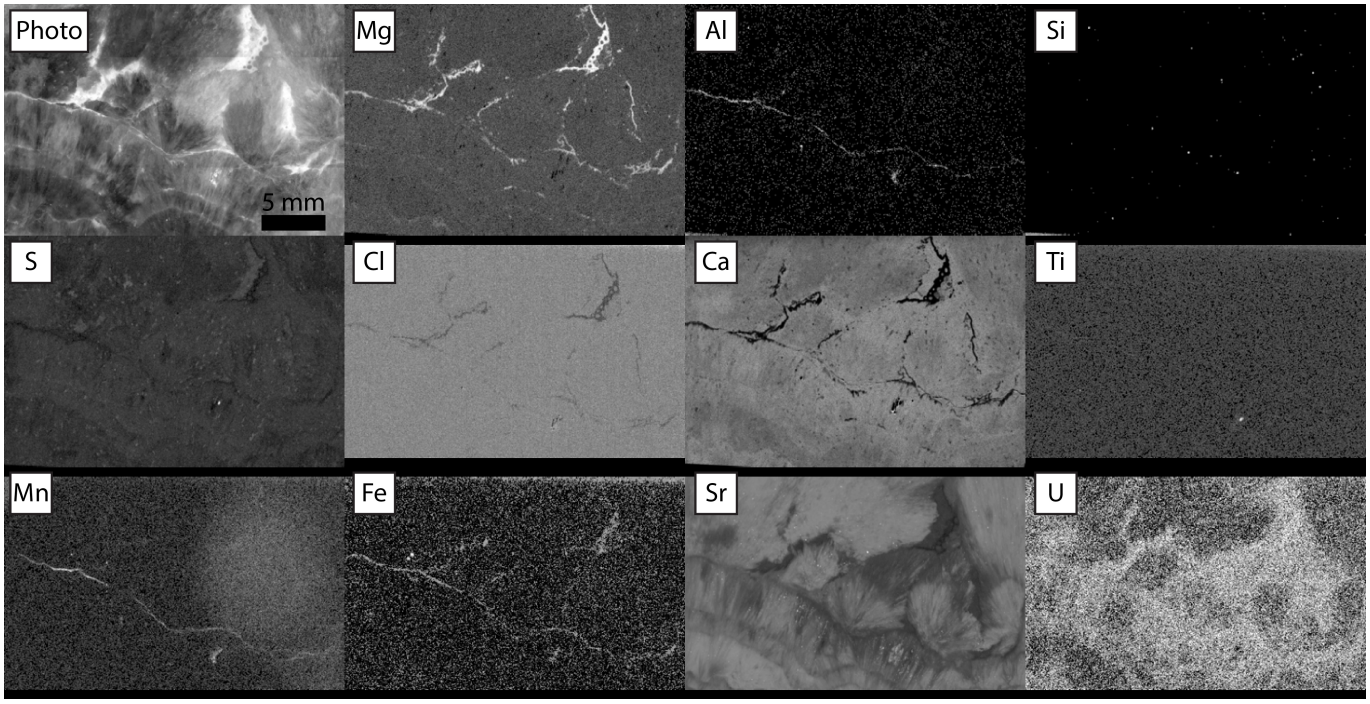

Figure 4. Relative intensities of emission regions for each element detected in Walnut Canyon, imaged at 20 μm pixels with 1.5 s.d. gaussian blur. Dwell time was 30 ms/pixel for maps with no incident radiation filter (Mg, Al, Si, S, Ca). Dwell time was 60 ms/pixel for maps with incident radiation filtered with 100 μm Al, 50 μm Ti, 20 μm Cu foil (Cl, Ti, Mn, Fe, Sr, U). Each panel is gamma and contrast adjusted to emphasize gradients between textures.

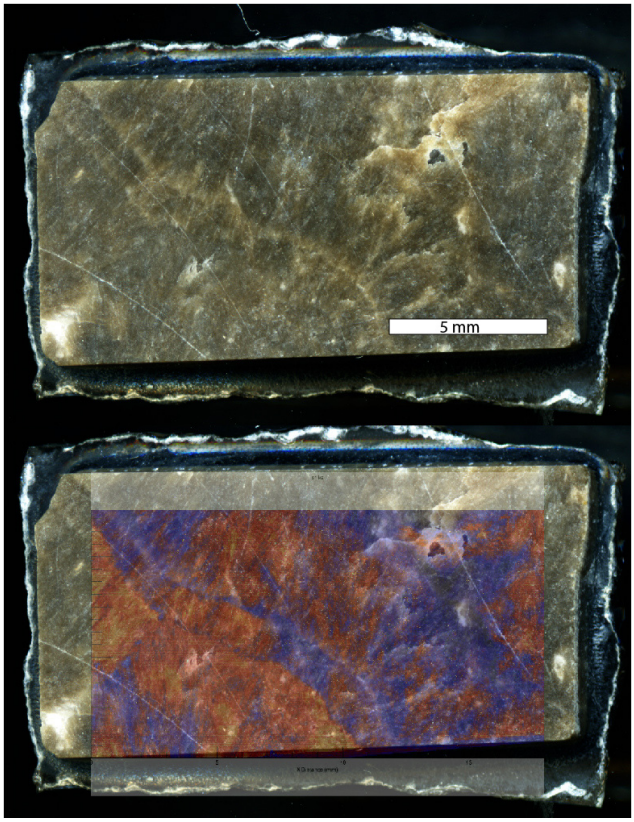

Figure 5. Synchrotron XRF Sr maps from beamline X26A NSLS Brookhaven National Lab overlain on the slab that was imaged. This XRF map was accomplished by on the fly scanning. To obtain U maps, we would have had to scan the same area above and below the binding energy for U and make a difference map because the SrKa peak is so large that the shoulder overlaps with the far less abundant UL3 peak. Still, based on the wealth of background information, we know that Sr is lost before U, so that focusing on botryoids with elevated Sr should produce the best areas for LAcarb reference material. This type of image can be registered for laser ablation so that only the most favorable areas are used as a reference material.

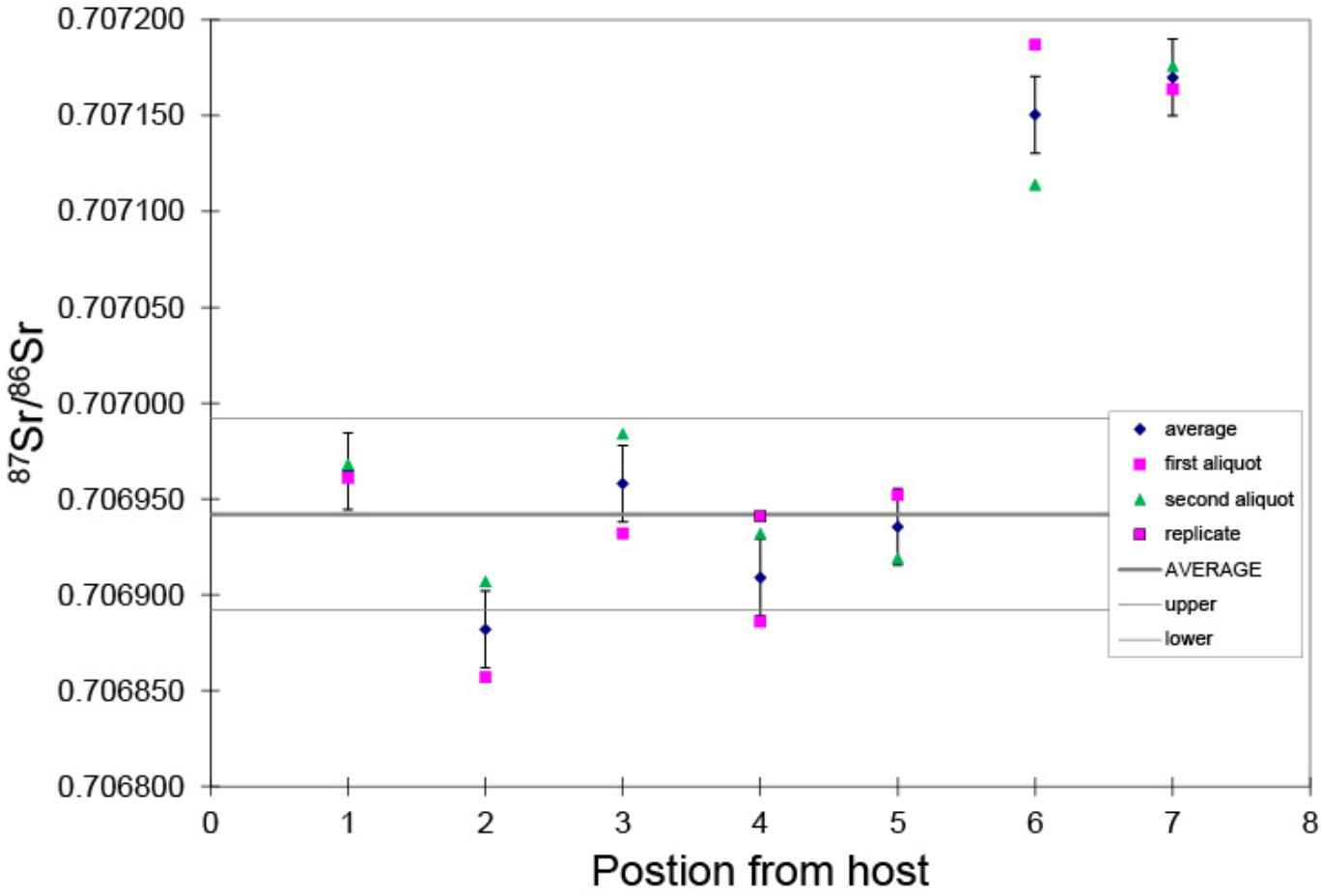

Figure 6. This graph shows Sr isotopes from the host to the center of the Neptunian dike. The aliquots were microsampled, dissolved and put through Sr spec resin, and run by Thermal Ionization Mass Spectrometry. The pink symbols represent two independent analyses from slabs that are quasi-equal distance from the host, and the blue is the average of those analyses. While showing variability, the dark brown calcite has $^{87}Sr/^{86}Sr$ like Capitanian seawater with an average of 1-5 of 0.706930(0.000069). The samples from positions 6 and 7 are a light brown color and a boundary is clearly visible in 6. These may represent later fluid alteration, or an extended marine cement history. This is presented because we suggest that this sample may also be a useful Sr isotope reference material. The slabs are about 0.5 cm across.

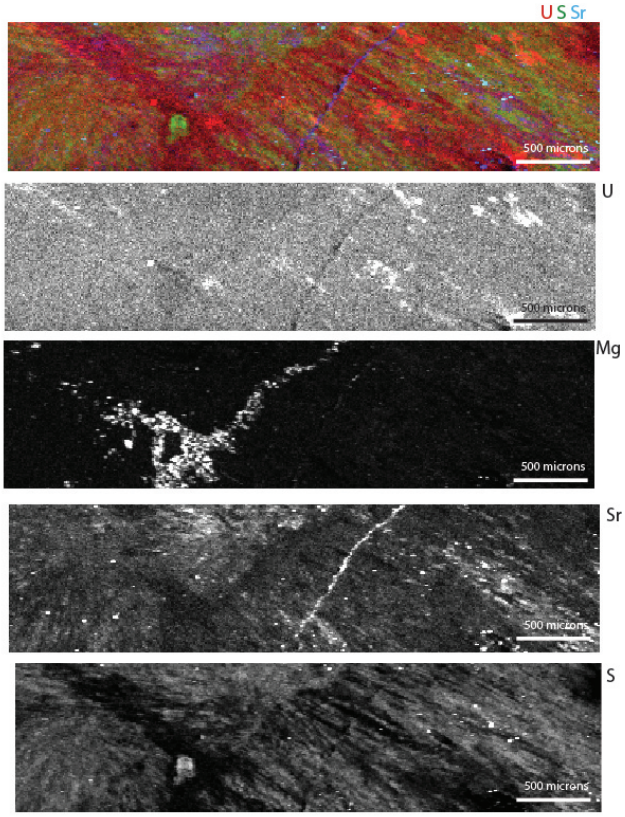

Figure 7. Tender Energy Range (TES) synchrotron XRF maps of the Walnut Canyon slab shown in Fig. 3-6. The panels are labeled with the elements they represent. The top map is a RGB map where red is U, green is S and blue is Sr (note scale bar on the bottom right of the RGB image is 100 microns). The brightest areas in the U map are artifacts from diffraction. The best preserved areas are an olive green.

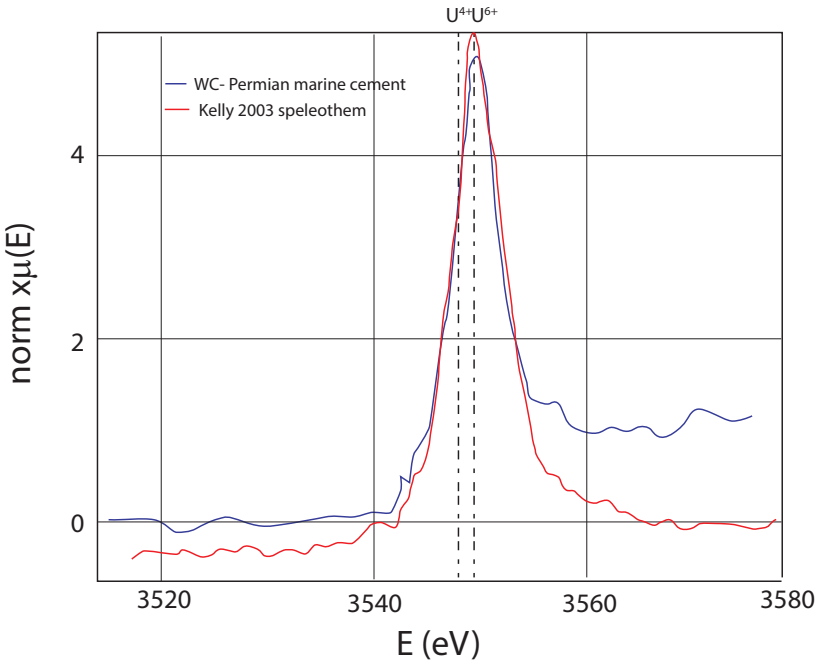

Figure 8. M5 edge X-ray absorption spectroscopy, 20 scans (15 s each) showing that uranium is in the oxidized state. The TES beamline has a monochrometer that is very stable, allowing hours worth of scanning without drift. Speleothem from a cave in Austria Kelly et al. (2003) that has U^{4+} for reference.

Figure 9. Hand specimen of a Barstow Formation tufa sample that is large enough to slab and share as a secondary LAcarb reference material.

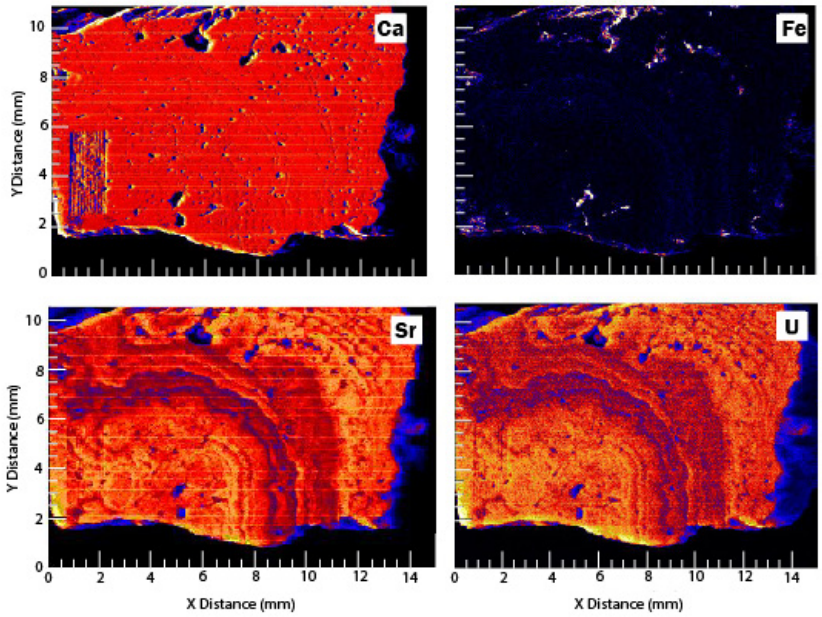

Figure 10. On the fly synchrotron XRF maps of Ca, Fe, Sr and U for a slab of Barstow tufa. This is from the same suite of samples being characterized for a LAcarb reference material, but it serves to show the relationships between U, Fe and Sr in the Barstow tufa samples.

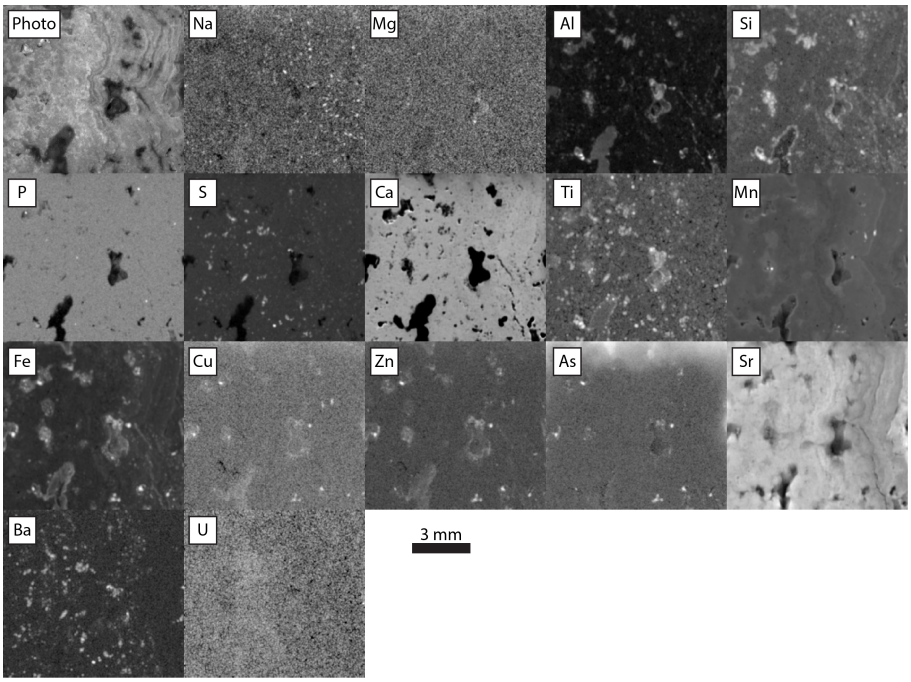

Figure 11. Relative intensities of emission regions for each element detected in Barstow tufa, imaged at 25 μm pixels with 400 ms/pixel dwell time and 1.5 s.d. gaussian blur. Each panel is gamma and contrast adjusted to emphasize gradients between textures. Na through Fe data collected with no incident radiation filter. Cu through U data collected with incident radiation filtered with 100 μm Al, 50 μm Ti, 20 μm Cu foil.

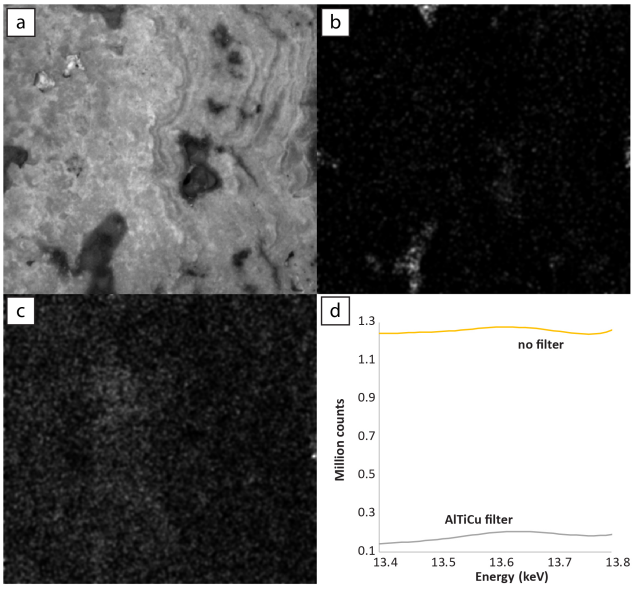

Figure 12. Comparison of U-L α maps of Barstow tufa, imaged at 25 µm pixels with 400 ms/pixel dwell time and 1.5 s.d. gaussian blur. (a) Sample image. (b) No incident radiation filter. (c) Incident radiation filtered with 100 µm Al, 50 µm Ti, 20 µm Cu foil. (d) Sum spectra of total counts in U-L α line region.

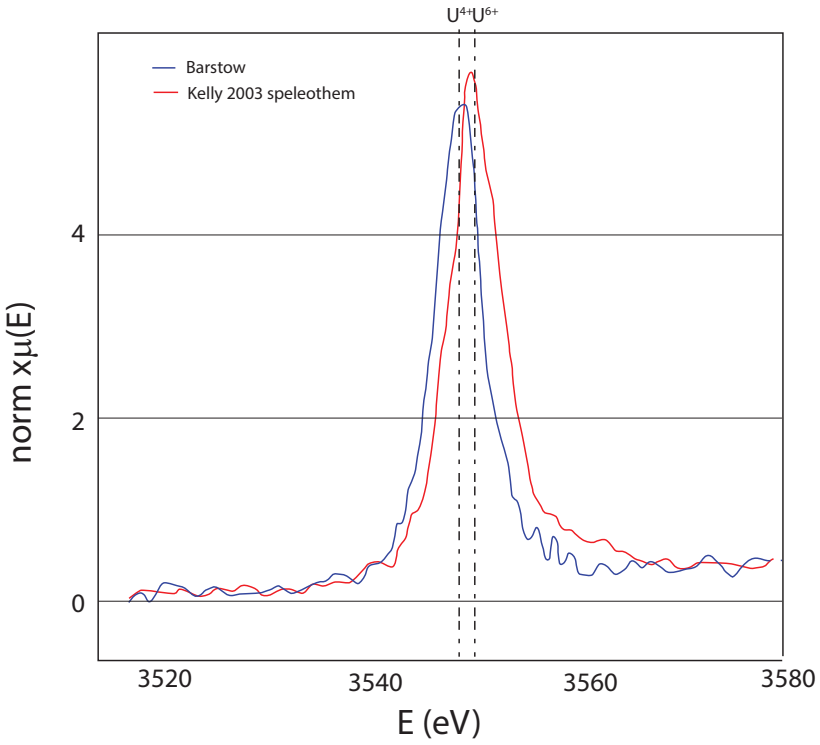

Figure 13. Uranium M5 edge spectroscopy showing that uranium is in the reduced state; for reference, the U^{6+} speleothem of (Kelly et al., 2003). Both measured at the TES beamline as described in Figure 9.

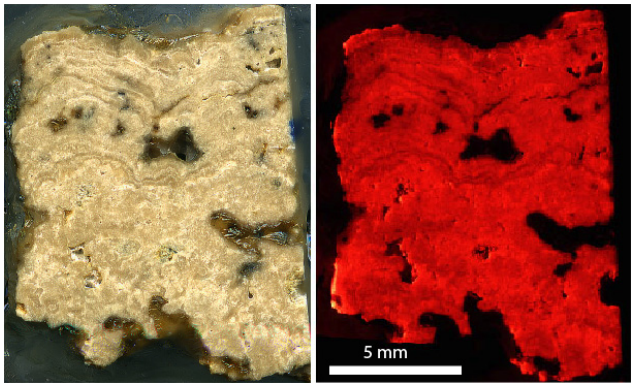

Figure 14. Slab from the Bartow Formation tufa sample that is being characterized for a possible secondary LAcarb standard. The fine laminae are like those described by Becker et al. (2001). The left image is a scan of the slab. The right image is a CL photomosaic from 360 images. Generally, the more micritic areas are brighter luminescence and the sparry layers have a duller luminescence.

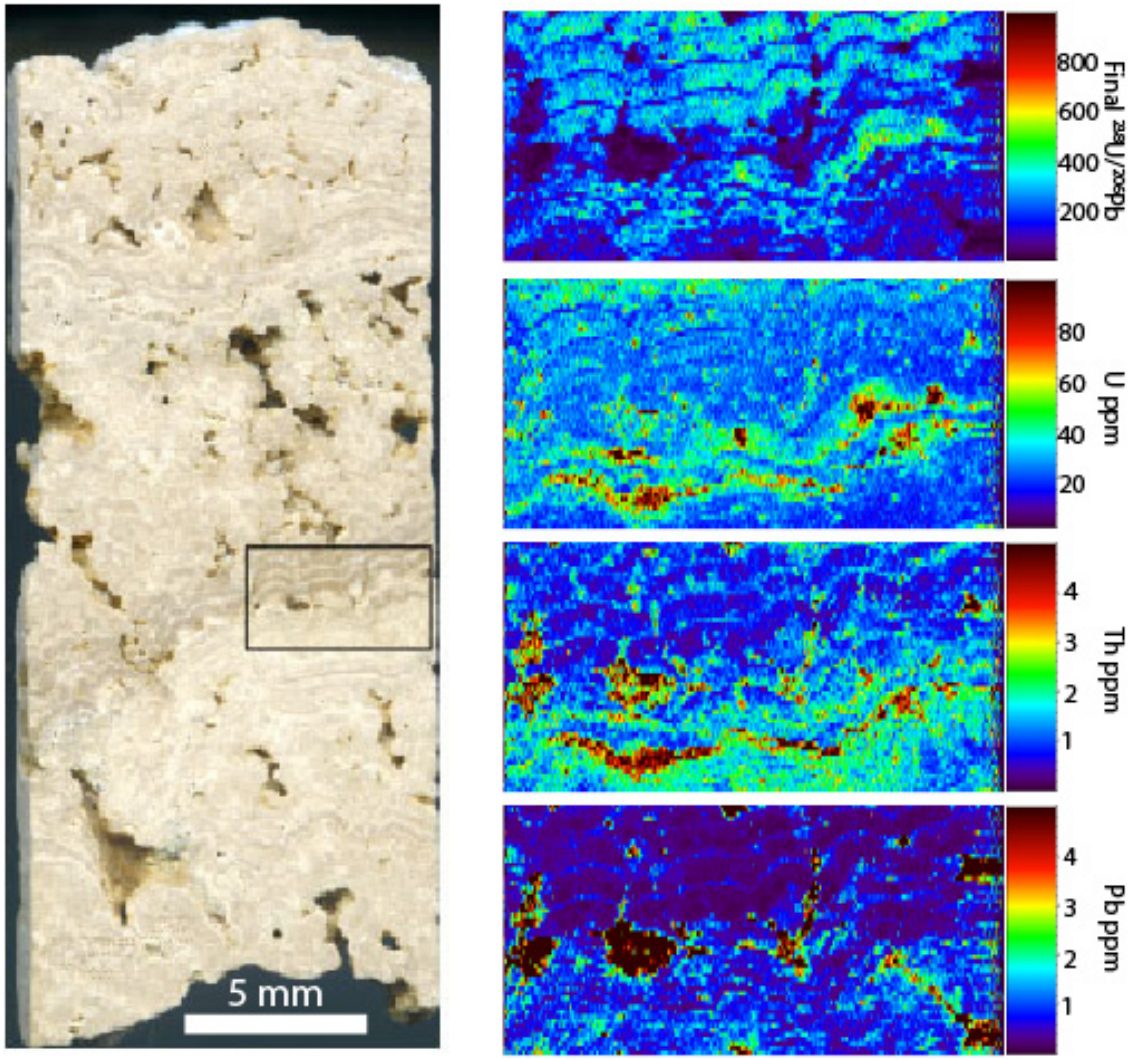

Figure 15. Slab of the Barstow tufa, approximately 1 cm wide. The box shows the location of the LA map which is approximately 5 mm wide. Note pores have high U, Th, and Pb concentrations but unfavorable U/Pb. The laminae have the most favorable U/Pb because Pb is lower, mostly less than 1 ppm.

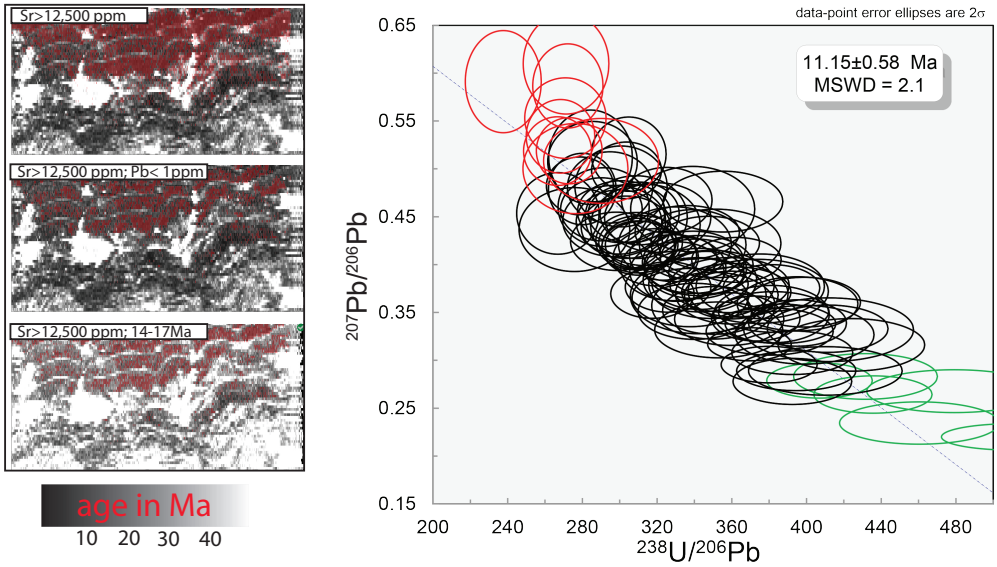

Figure 16. The base map for all is ^{238}U-^{206}Pb ages.This is the same map from Fig. 15 and is about 5 mm wide. In the top map, the red pixels are greater than 12,500 ppm Sr. Red pixels in the middle map also are greater than 12,500 ppm Sr plus the Pb concentration is less than 1 ppm. Red pixels in the lower map are greater than 12,500 ppm Sr and have an age range from 14-17 Ma with no correction for common Pb. The isochron plot is a binning of all of the red pixels from the second map (Sr concentrations grater than 12,500 ppm and Pb concentrations less than 1 ppm). Red and green data points represent the lower the low and high tails respectively.

Figure 17. Hand samples of the Turkana dolomite sample, both came from an area where carbonates were coating tree trunks. The big sample is from a very large cavity that was filled by calcite, then the yellow dolomite that is peeking out and finally by a coating of grey calcite. The smaller triangular shaped sample has a bark texture on the outside and appears to have precipitated in the cavity between three logs. The thickness of the dolomite layer is about 2 cm and it coats every surface in this paleo log pile. The small slabs come from the smaller of the two samples. The image on the left is the scanned slab used for XRF studies, and the one on the right is a CL photo mosaic with 459 photos.

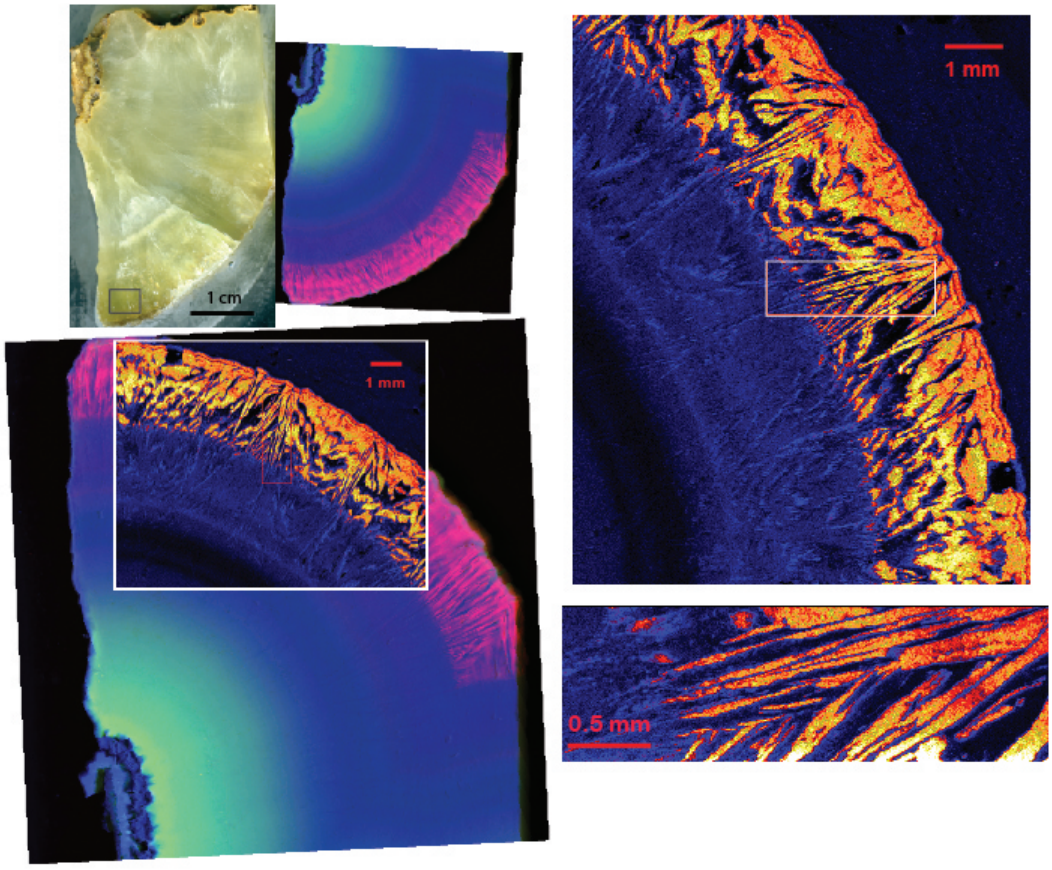

Figure 18. Slab of the dolomite with on the fly synchrotron XRF images. The rectangle at the bottom of the sample is the approximate location of the LA maps in Figure 21. Directly to the right of the slab image is a RGB (USrCa) map from beamline XFM at the NSLS II. The images on the right are maps of U from TES. On the lower left, the TES U map is overlain on the same area that was mapped at XFM. The XFM mapping was done at 17 keV with a 10 micron beam and a 10 micron step size, and a counting time of 0.1 seconds. The large TES map was made at 3550 eV with an 18 micron beam, 20 micron pixels, counted for 0.3 seconds. The detail map on the bottom right was also made at 3550 eV with a 4 micron beam, 3.75 micron pixels, counting for 0.3 seconds.

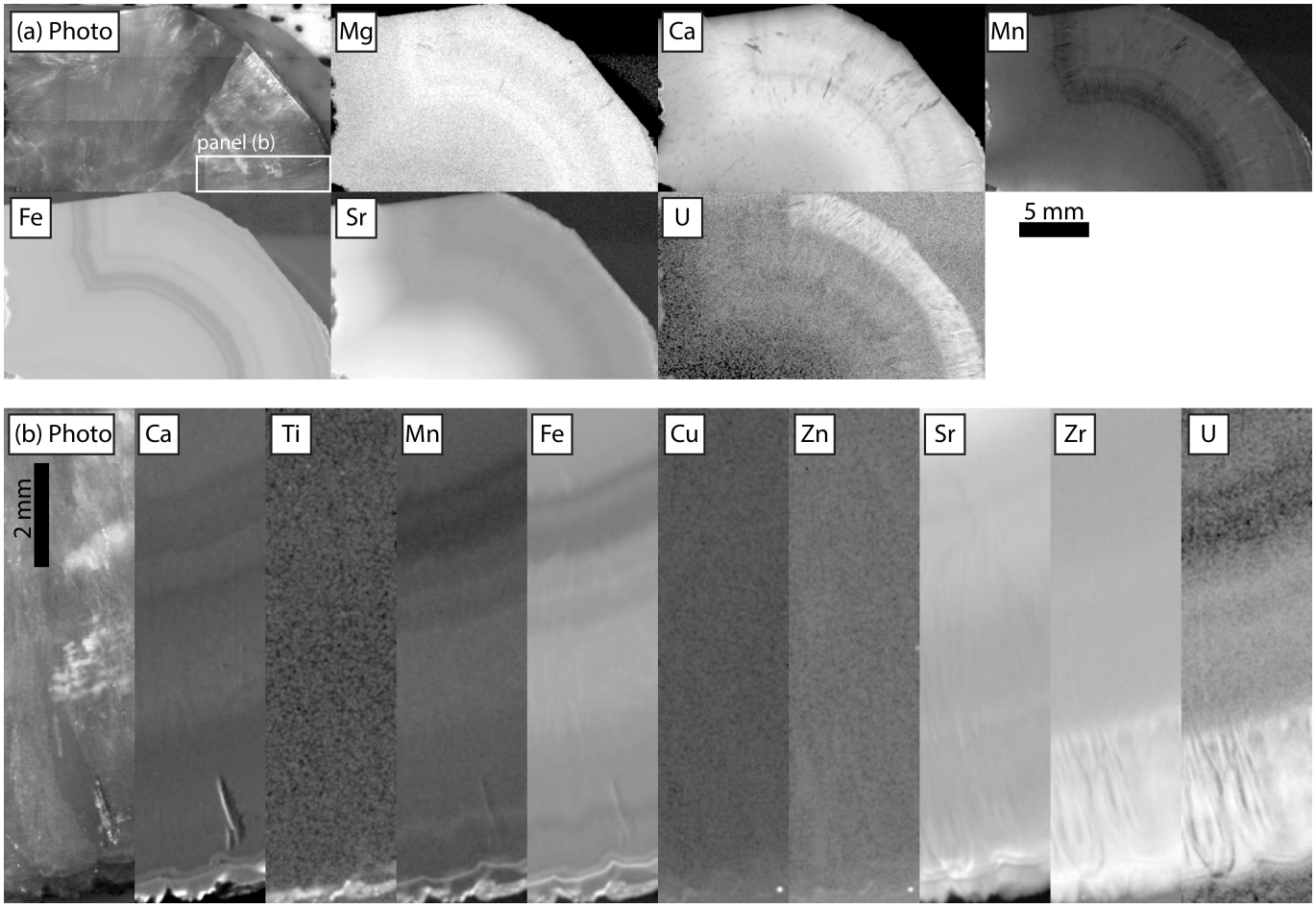

Figure 19. Relative intensities of emission regions for each element detected in Turkana Dolomite. Each panel is gamma and contrast adjusted to emphasize gradients between textures. (a) No incident radiation filter, imaged at 25 μm pixels with 120 ms/pixel dwell time and 1.5 s.d. gaussian blur, with box indicating region re-mapped with filter shown in panel b. (b) Incident radiation filtered using 100 μm Al, 50 μm Ti, 20 μm Cu foil, imaged at 20 μm pixels with 900 ms/pixel dwell time and 1.5 s.d. gaussian blur.

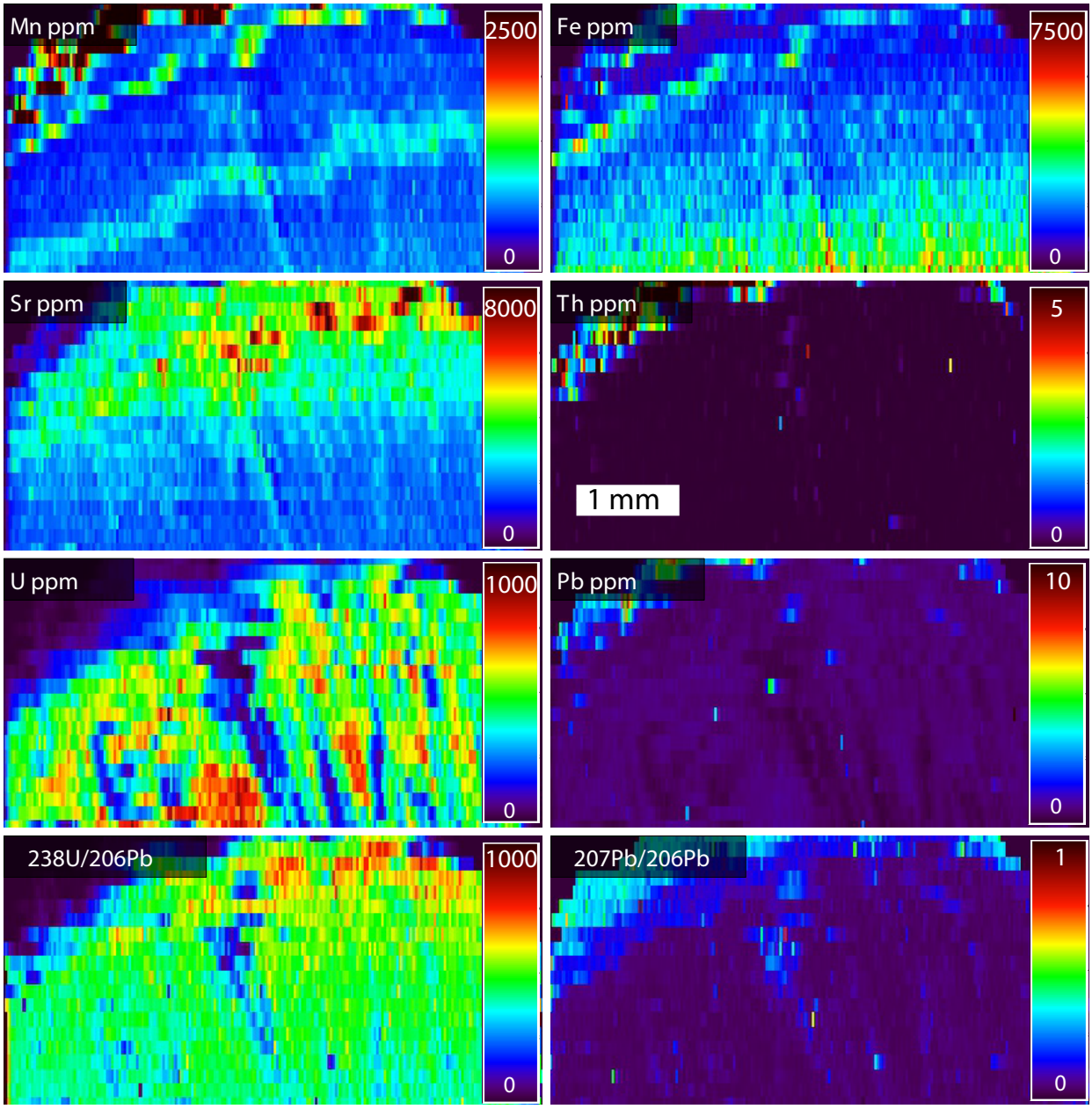

Figure 20. Laser Ablation ICPMS map of the TBW dolomite. The mapped area is from near the box shown in the slab on Fig. 18. The area mapped is approximately 5 mm wide. U is high concentration, while Pb and Th are low. The U/Pb ratio is very favorable.

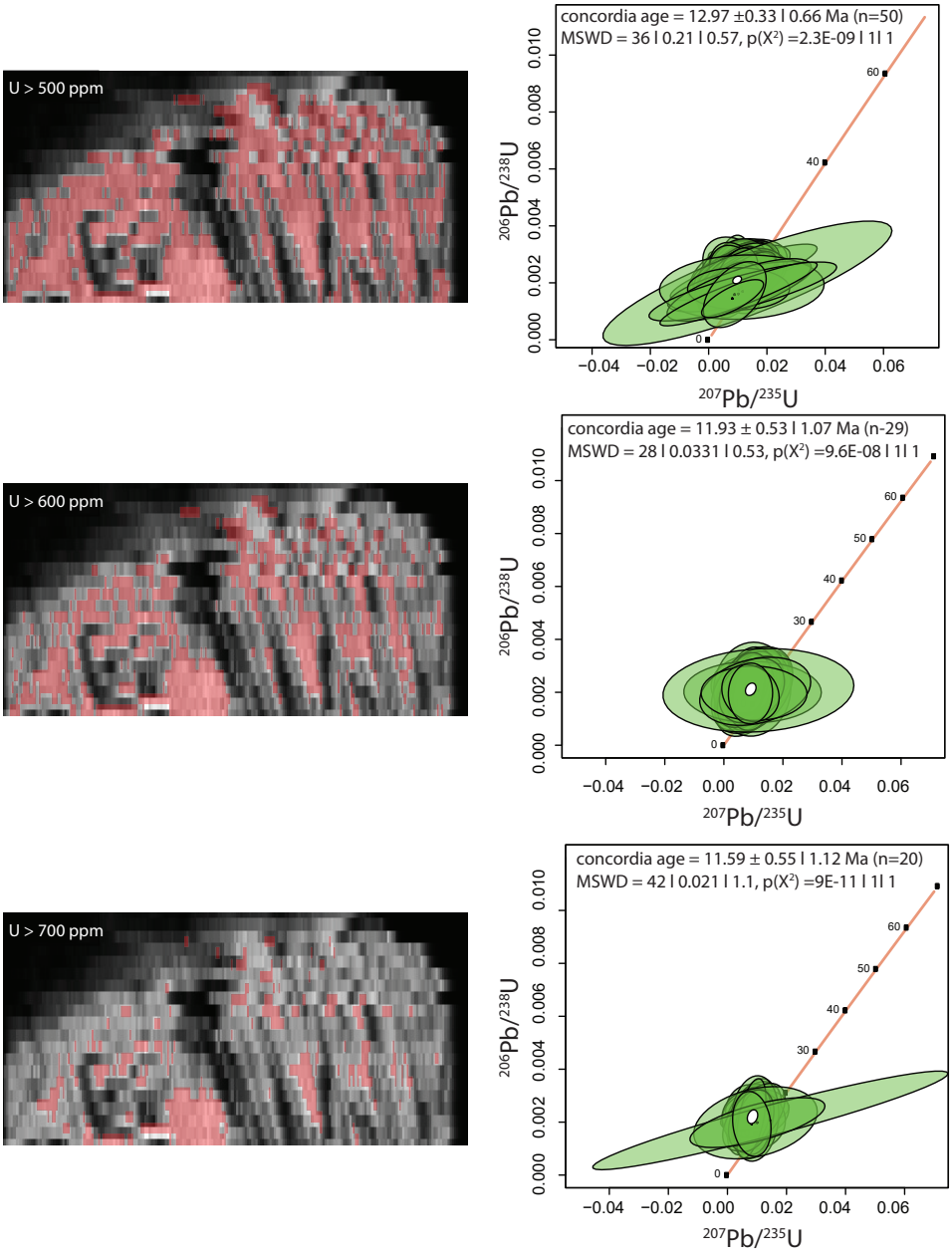

Figure 21. Map of U. Regions selected based on U concentration as noted on maps. Pooling pixels are based on U greater than 500, 600, and 700. The data are plotted in IsoplotR (Vermeesch, 2018). No corrections for Pb are made because we do not know if there is a bais between calcite and dolomite

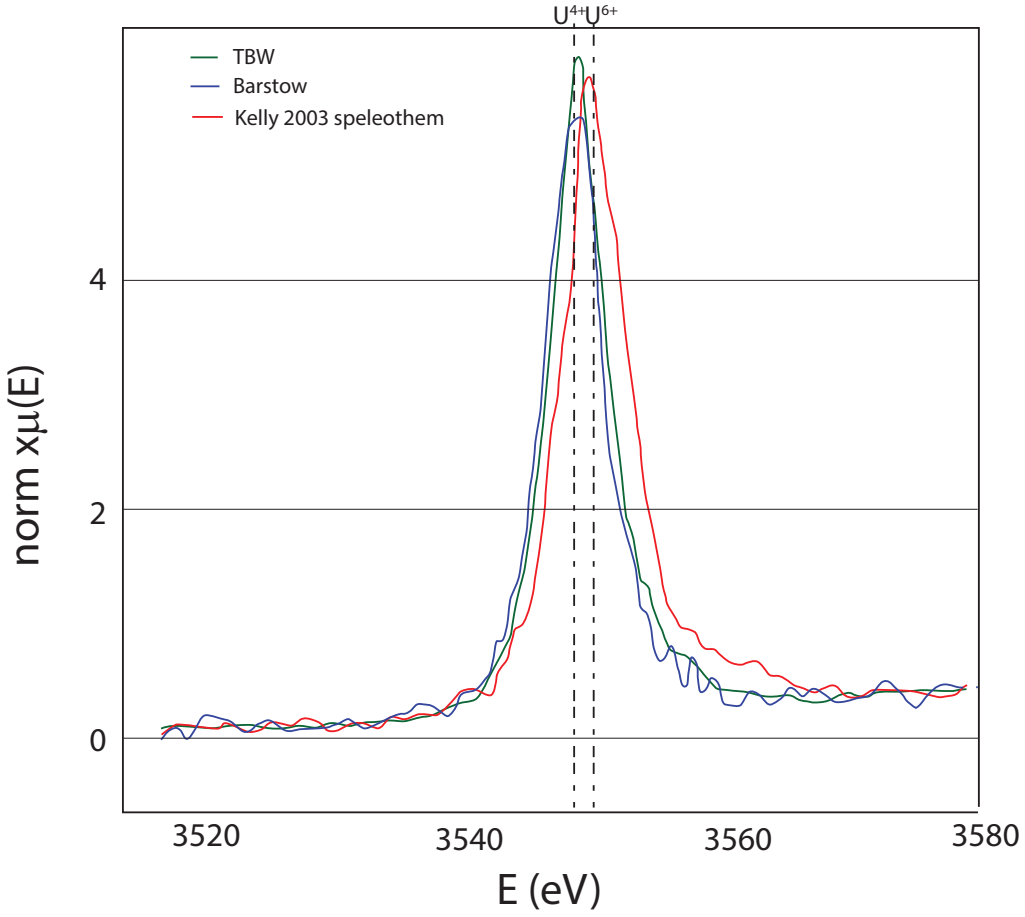

Figure 22. Uranium M5 edge spectroscopy of TBW sample showing that uranium is in the reduced state; for reference, the U^{6+} speleothem of Kelly et al. (2003). Both measured at the TES beamline as described in Figure 9.

Table 1. $^{87}Sr/^{86}Sr$ from aliquots of the Barstow tufa run by Thermal Ionization Mass Spectrometry

sample	$^{87}Sr/^{86}Sr$	2SD
BT1	0.720423	0.000011
BT2	0.721038	0.000011
BT3	0.719877	0.000011

Table 2. $^{87}Sr/^{86}Sr$ from aliquots of the Turkana dolomite run by Thermal Ionization Mass Spectrometry

sample	$^{87}Sr/^{86}Sr$	2SD
TBWi-1	0.703309	0.000011
TBWi-2	0.703299	0.000011
TBWo-1	0.703306	0.000011
TBWo-2	0.703312	0.000011